REPORT DOCUMENTATION PAGE

Form Approved OMB NO. 0704-0188

1. REPORT DATE (DD-MM-YYYY)	2. REPORT TYPE	3. DATES COVERED (From - To)
04-12-2013	Final Report	20-Aug-2009 - 19-Aug-2013

4. TITLE AND SUBTITLE
Oxygen Activation and Photoelectrochemical Oxidation on Oxide Surfaces

5a. CONTRACT NUMBER
W911NF-09-1-0426

5b. GRANT NUMBER

5c. PROGRAM ELEMENT NUMBER
611102

6. AUTHORS
Thomas J. Meyer, Aaron Vannucci, Zuofeng Chen, Wenjing Song, Animesh Nayak

5d. PROJECT NUMBER

5e. TASK NUMBER

5f. WORK UNIT NUMBER

7. PERFORMING ORGANIZATION NAMES AND ADDRESSES
University of North Carolina - Chapel Hill
Office of Sponsored Research
104 Airport Drive, Suite 2200, CB #1350
Chapel Hill, NC 27599 -1350

8. PERFORMING ORGANIZATION REPORT NUMBER

9. SPONSORING/MONITORING AGENCY NAME(S) AND ADDRESS (ES)
U.S. Army Research Office
P.O. Box 12211
Research Triangle Park, NC 27709-2211

10. SPONSOR/MONITOR'S ACRONYM(S)
ARO

11. SPONSOR/MONITOR'S REPORT NUMBER(S)
56714-CH.36

12. DISTRIBUTION AVAILIBILITY STATEMENT
Approved for Public Release; Distribution Unlimited

13. SUPPLEMENTARY NOTES
The views, opinions and/or findings contained in this report are those of the author(s) and should not contrued as an official Department of the Army position, policy or decision, unless so designated by other documentation.

14. ABSTRACT
Water oxidation catalysis by polypyridyl complexes of Ru(II) has been investigated mechanistically including studies in nonaqueous solvents with exploitation in electrocatalysis. Electrocatalysis studies have been extended to CO2 reduction to CO and, with added weak acids, to syngas (H2:CO) production and to CO2 splitting into CO and O2 based on a single catalyst. The reduction chemistry has been similarly extended to H2 production in a dye sensitized photoelectrosynthesis cell (DSPEC). Studies on DSPECs have been extended to the demonstration of accumulated multiple oxidative equivalents at surface catalysts on mesoporous TiO2 and to the exploration of the

15. SUBJECT TERMS
Water Oxidation Catalysis, Carbon Dioxide Reduction, Photoelectrochemical Hydrogen Generation, Dye Sensitized Photoelectrosynthesis Cell, Chromophore-Catalyst Assembly, Photoelectrochemistry

16. SECURITY CLASSIFICATION OF:			17. LIMITATION OF ABSTRACT	15. NUMBER OF PAGES	19a. NAME OF RESPONSIBLE PERSON
a. REPORT	b. ABSTRACT	c. THIS PAGE			Thomas Meyer
UU	UU	UU	UU		19b. TELEPHONE NUMBER: 919-843-8313

Report Title

Oxygen Activation and Photoelectrochemical Oxidation on Oxide Surfaces

ABSTRACT

Water oxidation catalysis by polypyridyl complexes of Ru(II) has been investigated mechanistically including studies in nonaqueous solvents with exploitation in electrocatalysis. Electrocatalysis studies have been extended to CO2 reduction to CO and, with added weak acids, to syngas (H2:CO) production and to CO2 splitting into CO and O2 based on a single catalyst. The reduction chemistry has been similarly extended to H2 production in a dye sensitized photoelectrosynthesis cell (DSPEC). Studies on DSPECs have been extended to the demonstration of accumulated multiple oxidative equivalents at surface catalysts on mesoporous TiO2 and to the exploration of the influence of Li+ doping. A new approach to surface-based assemblies based on phosphonate-derivatized porphyrins has been developed for creating antenna and chromophore-catalyst assembly structures by a layer-by-layer technique.

Enter List of papers submitted or published that acknowledge ARO support from the start of the project to the date of this printing. List the papers, including journal references, in the following categories:

(a) Papers published in peer-reviewed journals (N/A for none)

Received	Paper
08/27/2012 14.00	Wenjing Song, Zuofeng Chen, Christopher R. K. Glasson, Kenneth Hanson, Hanlin Luo, Michael R. Norris, Dennis L. Ashford, Javier J. Concepcion, M. Kyle Brennaman, Thomas J. Meyer. Interfacial Dynamics and Solar Fuel Formation in Dye-Sensitized Photoelectrosynthesis Cells, ChemPhysChem, (06 2012): 0. doi: 10.1002/cphc.201200100
08/27/2012 17.00	Dennis L. Ashford, David J. Stewart, Christopher R. Glasson, Robert A. Binstead, Daniel P. Harrison, Michael R. Norris, Javier J. Concepcion, Zhen Fang, Joseph L. Templeton, Thomas J. Meyer. An Amide-Linked Chromophore–Catalyst Assembly for Water Oxidation, Inorganic Chemistry, (06 2012): 6428. doi: 10.1021/ic300061u
08/27/2012 16.00	Aaron K. Vannucci, Zuofeng Chen, Javier J. Concepcion, Thomas J. Meyer. Nonaqueous Electrocatalytic Oxidation of the Alkylaromatic Ethylbenzene by a Surface Bound Ru, ACS Catalysis, (05 2012): 716. doi: 10.1021/cs300040m
08/27/2012 15.00	Christopher J. Gagliardi, Aaron K. Vannucci, Javier J. Concepcion, Zuofeng Chen, Thomas J. Meyer. The role of proton coupled electron transfer in water oxidation, Energy & Environmental Science, (01 2012): 7704. doi: 10.1039/c2ee03311a
08/31/2011 1.00	Zuofeng Chen, Paul G. Hoertz, Caleb A. Kent, Thomas J. Meyer. Application of High Surface Area Tin-Doped Indium Oxide Nanoparticle Films as Transparent Conducting Electrodes, Inorganic Chemistry, (09 2010): 8179. doi: 10.1021/ic100719r
08/31/2011 5.00	Wenjing Song, Christopher R. K. Glasson, Hanlin Luo, Kenneth Hanson, M. Kyle Brennaman, Javier J. Concepcion, Thomas J. Meyer. Photoinduced Stepwise Oxidative Activation of a Chromophore–Catalyst Assembly on TiO, The Journal of Physical Chemistry Letters, (07 2011): 1808. doi: 10.1021/jz200773r
08/31/2011 4.00	Wenjing Song, Zuofeng Chen, M. Kyle Brennaman, Javier J. Concepcion, Antonio Otávio T. Patrocinio, Neyde Y. Murakami Iha, Thomas J. Meyer. Making solar fuels by artificial photosynthesis, Pure and Applied Chemistry, (03 2011): 749. doi: 10.1351/PAC-CON-10-11-09
08/31/2011 3.00	Zuofeng Chen, Javier J. Concepcion, Hanlin Luo, Jonathan F. Hull, Amit Paul, Thomas J. Meyer. Nonaqueous Catalytic Water Oxidation, Journal of the American Chemical Society, (12 2010): 17670. doi: 10.1021/ja107347n
08/31/2011 2.00	Zuofeng Chen, Javier J. Concepcion, Thomas J. Meyer. Rapid catalytic water oxidation by a single site, Ru carbene catalyst, Dalton Transactions, (02 2011): 3789. doi: 10.1039/c0dt01178a
08/31/2012 21.00	Christopher Glasson, Javier Concepcion, Dennis Ashford, Wenjing Song, Patrick Holland, Thomas J Meyer. Self-Assembled Bilayers on Indium-Tin Oxide (SAB-ITO) Electrodes: A Design for Chromophore-Catalyst Photoanodes, Inorganic Chemistry, (08 2012): 8637. doi:
10/28/2011 11.00	Zuofeng Chen, Chuncheng Chen, David R. Weinberg, Peng Kang, Javier J. Concepcion, Daniel P. Harrison, Maurice S. Brookhart, Thomas J. Meyer. Electrocatalytic reduction of CO2 to CO by polypyridyl ruthenium complexes, Chemical Communications, (09 2011): 0. doi: 10.1039/c1cc15071e

11/02/2011 13.00 M. Kyle Brennaman, Antonio Otávio T. Patrocinio, Wenjing Song, Jonah W. Jurss, Javier J. Concepcion, Paul G. Hoertz, Matthew C. Traub, Neyde Y. Murakami?Iha, Thomas J. Meyer. Interfacial Electron Transfer Dynamics Following Laser Flash Photolysis of [Ru(bpy)2((4,4?-PO3H2)2bpy)]2+ in TiO2 Nanoparticle Films in Aqueous Environments,
ChemSusChem, (02 2011): 0. doi: 10.1002/cssc.201000356

12/04/2013 22.00 J. J. Concepcion, X. Hu, W. Yang, P. G. Hoertz, T. J. Meyer, Z. Chen. Concerted O atom-proton transfer in the O--O bond forming step in water oxidation,
Proceedings of the National Academy of Sciences, (04 2010): 0. doi: 10.1073/pnas.1001132107

12/04/2013 23.00 Zuofeng Chen, Javier J. Concepcion, Jonathan F. Hull, Paul G. Hoertz, Thomas J. Meyer. Catalytic water oxidation on derivatized nanoITO,
Dalton Transactions, (04 2010): 0. doi: 10.1039/c0dt00362j

12/04/2013 24.00 Z. Chen, A. K. Vannucci, J. J. Concepcion, J. W. Jurss, T. J. Meyer. Proton-coupled electron transfer at modified electrodes by multiple pathways,
Proceedings of the National Academy of Sciences, (12 2011): 0. doi: 10.1073/pnas.1115769108

12/04/2013 25.00 Z. Chen, J. J. Concepcion, M. K. Brennaman, P. Kang, M. R. Norris, P. G. Hoertz, T. J. Meyer. Splitting CO2 into CO and O2 by a single catalyst,
Proceedings of the National Academy of Sciences, (06 2012): 0. doi: 10.1073/pnas.1203122109

12/04/2013 26.00 Kenneth Hanson, Daniel A. Torelli, Aaron K. Vannucci, M. Kyle Brennaman, Hanlin Luo, Leila Alibabaei, Wenjing Song, Dennis L. Ashford, Michael R. Norris, Christopher R. K. Glasson, Javier J. Concepcion, Thomas J. Meyer. Self-Assembled Bilayer Films of Ruthenium(II)/Polypyridyl Complexes through Layer-by-Layer Deposition on Nanostructured Metal Oxides,
Angewandte Chemie International Edition, (12 2012): 0. doi: 10.1002/anie.201206882

12/04/2013 27.00 Dennis L. Ashford, Wenjing Song, Javier J. Concepcion, Christopher R. K. Glasson, M. Kyle Brennaman, Michael R. Norris, Zhen Fang, Joseph L. Templeton, Thomas J. Meyer. Photoinduced Electron Transfer in a Chromophore–Catalyst Assembly Anchored to TiO,
Journal of the American Chemical Society, (11 2012): 0. doi: 10.1021/ja3084362

12/04/2013 28.00 Christopher R. K. Glasson, Wenjing Song, Dennis L. Ashford, Aaron Vannucci, Zuofeng Chen, Javier J. Concepcion, Patrick L. Holland, Thomas J. Meyer. Self-Assembled Bilayers on Indium–Tin Oxide (SAB-ITO) Electrodes: A Design for Chromophore–Catalyst Photoanodes,
Inorganic Chemistry, (08 2012): 0. doi: 10.1021/ic300636w

12/04/2013 29.00 Zuofeng Chen, Thomas J. Meyer. Copper(II) Catalysis of Water Oxidation,
Angewandte Chemie, (01 2013): 0. doi: 10.1002/ange.201207215

12/04/2013 30.00 Kenneth Hanson, M. Kyle Brennaman, Akitaka Ito, Hanlin Luo, Wenjing Song, Kelsey A. Parker, Rudresh Ghosh, Michael R. Norris, Christopher R. K. Glasson, Javier J. Concepcion, Rene Lopez, Thomas J. Meyer. Structure–Property Relationships in Phosphonate-Derivatized, Ru,
The Journal of Physical Chemistry C, (07 2012): 0. doi: 10.1021/jp304088d

12/04/2013 31.00 Zuofeng Chen, Peng Kang, Ming-Tian Zhang, Brian R. Stoner, Thomas J. Meyer. Cu(ii)/Cu(0) electrocatalyzed CO2 and H2O splitting,
Energy & Environmental Science, (01 2013): 0. doi: 10.1039/c3ee24487c

12/04/2013 32.00 Hanlin Luo, Wenjing Song, Paul G. Hoertz, Kenneth Hanson, Rudresh Ghosh, Sylvie Rangan, M. Kyle Brennaman, Javier J. Concepcion, Robert A. Binstead, Robert Allen Bartynski, Rene Lopez, Thomas J. Meyer. A Sensitized Nb2O5 Photoanode for Hydrogen Production in a Dye-Sensitized Photoelectrosynthesis Cell,
Chemistry of Materials, (01 2013): 0. doi: 10.1021/cm3027972

12/04/2013 33.00 Ming-Tian Zhang, Zuofeng Chen, Peng Kang, Thomas J. Meyer. Electrocatalytic Water Oxidation with a Copper(II) Polypeptide Complex,
Journal of the American Chemical Society, (02 2013): 0. doi: 10.1021/ja3097515

12/04/2013 34.00 Wenjing Song, Hanlin Luo, Kenneth Hanson, Javier J. Concepcion, M. Kyle Brennaman, Thomas J. Meyer. Visualization of cation diffusion at the TiO2 interface in dye sensitized photoelectrosynthesis cells (DSPEC),
Energy & Environmental Science, (02 2013): 0. doi: 10.1039/c3ee24184j

12/04/2013 35.00 Zuofeng Chen, Christopher R. K. Glasson, Patrick L. Holland, Thomas J. Meyer. Electrogenerated polypyridyl ruthenium hydride and ligand activation for water reduction to hydrogen and acetone to iso-propanol,
Physical Chemistry Chemical Physics, (05 2013): 0. doi: 10.1039/c3cp51946e

TOTAL: **26**

Number of Papers published in peer-reviewed journals:

(b) Papers published in non-peer-reviewed journals (N/A for none)

Received Paper

TOTAL:

Number of Papers published in non peer-reviewed journals:

(c) Presentations

Number of Presentations: 0.00

Non Peer-Reviewed Conference Proceeding publications (other than abstracts):

Received Paper

TOTAL:

Number of Non Peer-Reviewed Conference Proceeding publications (other than abstracts):

Peer-Reviewed Conference Proceeding publications (other than abstracts):

Received	Paper

TOTAL:

Number of Peer-Reviewed Conference Proceeding publications (other than abstracts):

(d) Manuscripts

Received	Paper
08/27/2012 19.00	Kenneth Hanson, Daniel Torelli, Aaron Vannucci, Matthew Kyle Brennaman, Hanlin Luo, Leila Alibabaei, Wenjing Song, Dennis Ashford, Michael Norris, Christopher Glasson, Javier Concepcion, Thomas J. Meyer. Self-assembled Bilayer Films of Ru(II) Polypyridyl Complexes by Layer-by-Layer Deposition on High-Surface Area Metal Oxides, Angewandte Chemie (08 2012)
08/31/2012 20.00	Hanlin Luo, Wenjing Song, Paul G. Hoertz, Kenneth Hanson, Rudresh Ghosh, Sylvie Rangan, M. Kyle Brennaman, Javier J. Concepcion, Robert A. Binstead, Robert Allen Bartynski, Rene Lopez, Thomas J. Meyer. A Sensitized Nb2O5 Photoanode for Hydrogen Production in a Dye-Sensitized Photoelectrosynthesis Cell, Chemistry of Materials (08 2012)
09/01/2011 8.00	Zuofeng Chen, Aaron Vannucci , Thomas Meyer . Proton coupled electron transfer at modified electrodes. Multiple pathways. , Proceedings of the National Academy of Sciences(US) (12 2011)
09/01/2011 9.00	Zuofeng Chen, Chuncheng Chen , David Weinberg, Peng Kang, Javier Concepcion . Electrocatalytic Reduction of CO2 to CO by Polypyridyl Ruthenium Complexes, Chem. Commun. (09 2011)
09/01/2011 10.00	Zuofeng Chen, Thomas Meyer, et al. Electrochemical and Solar Splitting of CO2 into CO and O2. One Catalyst is Enough, IN PREP (09 2011)

TOTAL: **5**

Number of Manuscripts:

Books

Received	Paper

TOTAL:

Patents Submitted

Patents Awarded

Awards

Porter Medal, European Photochemical Association, Inter-American Photochemical Society, and the Asian and Oceanian Photochemical Association (2012)

Kosolapoff Award, Auburn Unversity (2012)

Honorary Doctor of Chemistry, Ohio University (May, 2013)

Honda-Fujishima Lectureship Award sponsored by the Japan Photochemical Association (September, 2013)

Graduate Students

NAME	PERCENT_SUPPORTED
FTE Equivalent:	
Total Number:	

Names of Post Doctorates

NAME	PERCENT_SUPPORTED
Zuofeng Chen	0.50
Christopher Glasson	0.50
Animesh Nayak	0.50
Wenjing Song	0.50
Aaron Vannucci	0.50
FTE Equivalent:	**2.50**
Total Number:	**5**

Names of Faculty Supported

NAME	PERCENT_SUPPORTED
FTE Equivalent:	
Total Number:	

Names of Under Graduate students supported

NAME	PERCENT_SUPPORTED

FTE Equivalent:
Total Number:

Student Metrics

This section only applies to graduating undergraduates supported by this agreement in this reporting period

The number of undergraduates funded by this agreement who graduated during this period:	0.00
The number of undergraduates funded by this agreement who graduated during this period with a degree in science, mathematics, engineering, or technology fields:.....	0.00
The number of undergraduates funded by your agreement who graduated during this period and will continue to pursue a graduate or Ph.D. degree in science, mathematics, engineering, or technology fields:.....	0.00
Number of graduating undergraduates who achieved a 3.5 GPA to 4.0 (4.0 max scale):.....	0.00
Number of graduating undergraduates funded by a DoD funded Center of Excellence grant for Education, Research and Engineering:.....	0.00
The number of undergraduates funded by your agreement who graduated during this period and intend to work for the Department of Defense	0.00
The number of undergraduates funded by your agreement who graduated during this period and will receive scholarships or fellowships for further studies in science, mathematics, engineering or technology fields:	0.00

Names of Personnel receiving masters degrees

NAME

Total Number:

Names of personnel receiving PHDs

NAME

Total Number:

Names of other research staff

NAME	PERCENT_SUPPORTED

FTE Equivalent:
Total Number:

Sub Contractors (DD882)

Inventions (DD882)

Scientific Progress

Table of Contents:

See Attachments Below

Technology Transfer

Oxygen Activation and Photoelectrochemical Oxidation on Oxide Surfaces
Agreement Number: W911NF0910426
Final Report

Foreword:

This report summarizes research findings based on Army Research Office support from August 20, 2009 to August 19, 2013 on grant W911NF0910426.

1. Water Oxidation Catalysts

Significant progress in water oxidation catalysis has been made with single-site Ru metal complex catalysts such as $[Ru(Mebimpy)(bpy)(OH_2)]^{2+}$ (**1**) (Mebimpy = 2,6-bis(1-methylbenzimidazol-2-yl)pyridine; bpy = 2,2'-bipyridine) in solution or on oxide surfaces with $[Ru(Mebimpy)(4,4'\text{-}((HO)_2OPCH_2)_2bpy)(OH_2)]^{2+}$ where 4,4'-$((HO)_2OPCH_2)_2$bpy is 4,4'-bis-methlylenephosphonato-2,2'-bipyridine) (**1-PO_3H_2**) bound to ITO and *nano*ITO electrodes as shown in Scheme 1.1. The overall mechanism in Scheme 1.1 has been established by mixing experiments with spectrophotometric monitoring. The key O–O bond forming step, analyzed by quantum mechanical simulations (QM/MM), features O-atom attack of Ru^{V}=O on a H_2O molecule. Kinetic studies have identified a new pathway which utilizes added bases as proton acceptors and concerted atom-proton transfer (APT) in which O-atom transfer from the water molecule occurs in concert with proton transfer to added base (B), eq. 1.1, with considerable rate enhancements. A new a pathway was also identified in which O-atom transfer to OH^- occurs (eq. 1.1a) under basic conditions with a kinetic rate increase of 10^6 compared to water oxidation in acid. These results have important implications for catalytic, electrocatalytic, and photoelectrocatalytic water oxidation.

Scheme 1.1. Water oxidation mechanism for *nano*ITO|1-PO_3H_2.

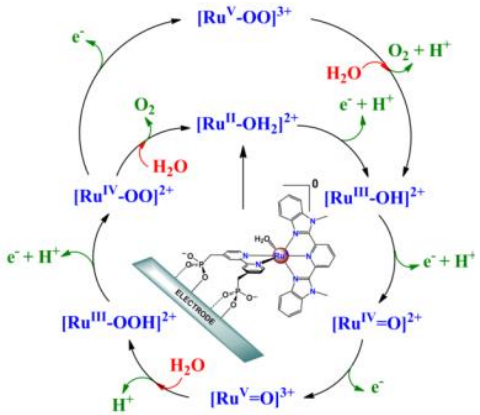

$$Ru^{V}{=}O^{3+}\text{---}O\begin{matrix}H\\ H^{+}\\ H\text{–}B\end{matrix} \longrightarrow Ru^{III}\text{-}OOH^{2+} + HB \quad (1.1)$$

$$-Ru^{V}{=}O^{3+} + OH^{-} \rightarrow -Ru^{III}\text{-}OOH^{2+} \quad (1.1a)$$

Electrode Materials

Our catalysts are used in a heterogeneous catalytic system on prepared, optically transparent, conducting nanoparticles of tin-doped indium oxide (ITO), which we have termed nanoITO. Figure 1.1 shows scanning electron microscope images of the electrode materials. After fabrication, the electrodes are derivatized with surface-bound molecular catalysts at levels comparable to TiO_2 electrodes used in conventional Dye Sensitized Solar Cells (DSSC). The conductivity of the electrodes provides a basis for facile interfacial electron transfer and rapid, reversible, potential controlled color changes. This allows for direct spectral (rather than current) monitoring of voltammograms, and multi-layer catalysis of surface redox reactions.

*Nano*ITO electrodes are prepared by spin-coating suspensions of ~40 nm ITO nanoparticles onto planar substrates (e.g. borosilicate glass, quartz, FTO (fluoride-doped SnO_2), or ITO). Once formed, films were annealed in air at 500 ^{o}C for 1 hour and then at 300 ^{o}C under 3% H_2/N_2 for an additional hour. Thickness was controlled by varying nanoparticle concentration in the suspension: 0.55 μm for 12 wt%, 2.5 μm for 22 wt%, 6.7 μm for 29 wt%, and 15.7 μm for 36 wt%. Top-down and cross-sectional field emission scanning electron microscope (FESEM) images demonstrate that the films are highly porous and uniform, allowing for the diffusion of solvent and electrolyte within the porous film structure, Figure 1.1.[1]

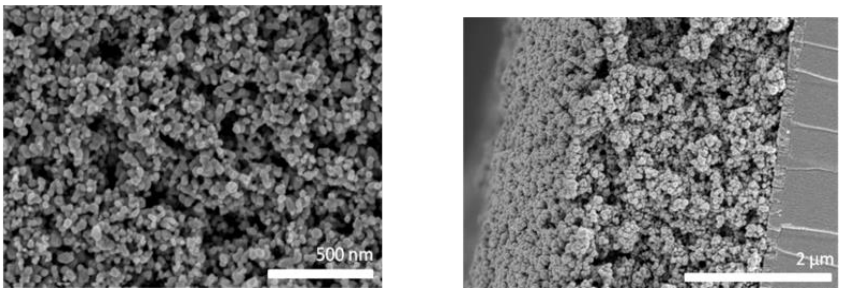

Figure 1.1. Top-down (left) and cross-sectional (right) field emission scanning electron microscopy (FESEM) images of an ITO|*nano*ITO slide (2.5 μm) annealed in air at 500 ^{o}C and under a steady flow of 3% H_2/N_2 at 300 ^{o}C. For both images, a thin coating of Au/Pd was deposited prior to imaging.

It has been shown that redox potentials, pH dependences, catalytic properties, and water oxidation mechanism are all retained on oxide surfaces. We have obtained greatly enhanced rates for **1-PO_3H_2** on the surface of conductive *nano*ITO films under basic conditions and shown that surface binding provides a basis for sustained, electrocatalytic water oxidation over an extended pH range. We also used direct spectrophotometric monitoring to provide direct evidence for surface mechanism and observation of catalytic intermediates, eqs (1.2)-(1.9) and Figure 1.2.

(1.2) $Ru^{II}\text{-}OH_2^{2+} - e^- \rightarrow Ru^{III}\text{-}OH_2^{3+}$

(1.3) $Ru^{III}\text{-}OH_2^{3+} - 2H^+ - e^- \rightarrow Ru^{IV}{=}O^{2+}$

(1.4) $Ru^{IV}{=}O^{2+} - e^- \rightarrow Ru^{V}{=}O^{3+}$ and the following water oxidation cycle

(1.5) $Ru^{IV}(OO)^{2+}$ as a stable intermediate on the surface

(1.6) $Ru^{IV}=O^{2+} + 2H^+ + e^- \rightarrow Ru^{III}\text{-}OH_2^{3+}$

(1.7) $Ru^{III}\text{-}OH_2^{3+} + e^- \rightarrow Ru^{II}\text{-}OH_2^{2+}$

(1.8) $Ru^{IV}(OO)^{2+} + H^+ + e^- \rightarrow Ru^{III}\text{-}OOH^{2+}$

(1.9) $Ru^{III}\text{-}OOH^{2+} + H^+ + e^- \rightarrow Ru^{II}(HOOH)^{2+}$

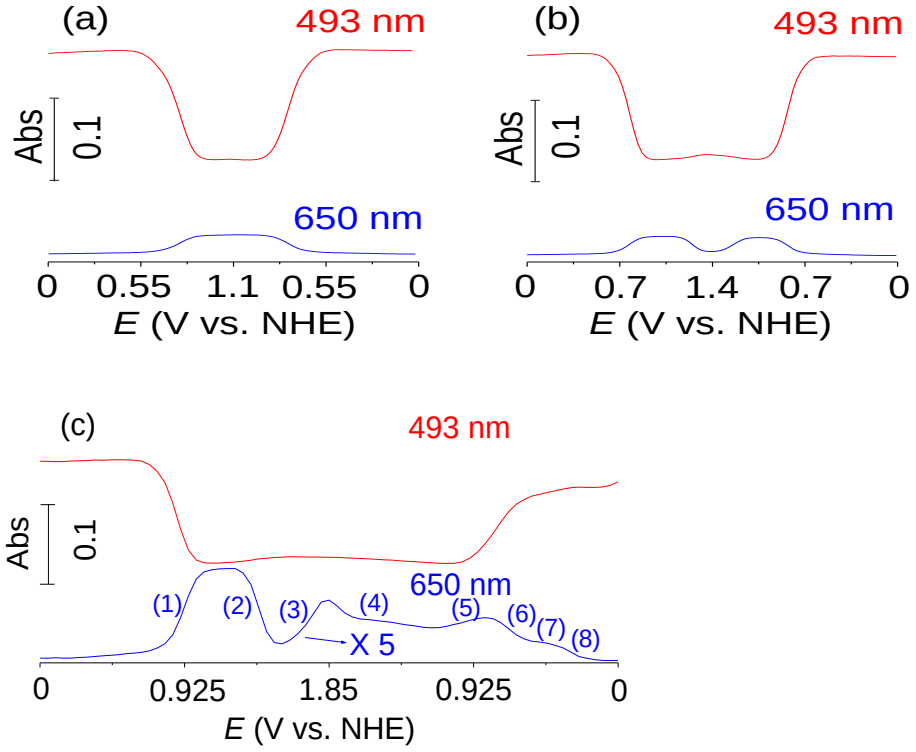

Figure 1.2. Spectral evolution of surface-bound 1-PO_3H_2, ITO|*nano*ITO|1-PO_3H_2, at pH 1 (0.1 M HNO_3) during CV scans between: (a) 0 - 1.1 V, (b) 0 - 1.4 V, and (c) 0 - 1.85 V. The monitoring wave lengths were λ_{max} = 493 nm for $Ru^{II}\text{-}OH_2^{2+}$ and $Ru^{II}(HOOH)^{2+}$ (red line), and λ_{max} = 650 nm for $Ru^{III}\text{-}OH_2^{3+}$ and $Ru^{III}\text{-}OOH^{2+}$ (blue line). Scan rate, 10 mV/s. For clarity, the blue line in (c) was magnified by 5-fold. The sequence of electrochemical/chemical events was keyed to the scheme above and steps (2)-(9).

Water Oxidation Mechanism

The mechanism of interfacial water oxidation by [Ru(Mebimpy)(4,4'-$((HO)_2OPCH_2)_2$bpy)(OH_2)]$^{2+}$ (Mebimpy is 2,6-bis(1-methylbenzimidazol-2yl) and 4,4'-$((HO)_2OPCH_2)_2$bpy is 4,4'-bis-methlylenephosphonato-2,2'-bipyridine) (**1-PO_3H_2**) bound to ITO and nanoITO electrodes is shown in Scheme 1.1. Key elements in the mechanism include stepwise proton coupled electron transfer (PCET) oxidation from nanoITO|$Ru\text{-}OH_2^{2+}$ to higher oxidation states $Ru^{IV}=O^{2+}$ and $Ru^{V}=O^{3+}$. This process occurs through $Ru^{III}\text{-}OH^{2+}$ or $Ru^{III}\text{-}OH_2^{3+}$ with a pK_a = 2.3 for the latter. In acidic solutions, oxidative activation from $Ru^{III}\text{-}OH^{2+}$/$Ru^{III}\text{-}OH_2^{3+}$ occurs through $Ru^{IV}(OH)^{3+}$. Further oxidation to $Ru^{V}=O^{3+}$ followed by O-atom transfer from H_2O

gives Ru^{III}-OOH^{3+}, which can be further oxidized to the peroxide $Ru^{IV}(OO)^{2+}$ followed by slow O_2 evolution. Additional oxidation of the Ru^{IV} peroxide to $Ru^{V}(OO)^{3+}$ increases the lability of O_2 leading to re-entry into the catalytic cycle through O_2 loss and regeneration of Ru^{III}-OH^{2+}. Evidence has been obtained for intermediate $Ru^{IV}(OO)^{2+}$/Ru^{III}-OOH^{2+} and Ru^{III}-OOH^{2+}/$Ru^{II}(HOOH)^{2+}$ couples both in solution and on electrode surfaces.

A kinetic bottleneck to water oxidation occurs in the oxidation of Ru^{III}-OH^{2+} to Ru^{IV}=O^{2+}, Scheme 1.1. It arises from the large difference in pK_a values between Ru^{III}-OH^{2+} (> 14) and Ru^{IV}=OH^{3+} (< 0). We have investigated Ru^{III}-OH^{2+} or Ru^{III}-OH_2^{3+} ↔ Ru^{IV}=O^{2+} interconversion on the surfaces of metal oxide electrodes by a combination of electrochemical and spectroelectrochemical measurements under a variety of conditions. In these experiments, the phosphonate-derivatized water oxidation catalyst, $Ru(Mebimpy)(4,4'\text{-}(PO_3H_2CH_2)_2bpy)(OH_2)]^{2+}$, shown in Scheme 1.1, was attached to the surfaces of three metal oxides: planar FTO (fluoride-doped SnO_2) and nanostructured, mesoporous films of ITO (nanoITO) both of which are conductive and function as electrodes, and nanostructured films of TiO_2 (nanoTiO_2) which is a semiconductor. The results that we have obtained are revealing. They demonstrate participation by multiple pathways on the surface whose relative importance varies depending on solution composition, the nature of electrode, the extent of catalyst loading, and temperature. Pathways have been identified for direct, Ru^{III}-OH^{2+} – e^- → Ru^{IV}=OH^{3+} oxidation, indirect oxidation by cross-surface disproportionation of Ru^{III}-OH^{2+}, and concerted electron-proton transfer (EPT) with added acetate anion, equation 1.1. In propylene carbonate as solvent, evidence has been found for proton transfer to the surface-bound phosphonate groups and generalized solvation effects arising, for example, from loss of solvation energy for released protons. Reduction of Ru^{IV}=O^{2+} to Ru^{III}-OH_2^{3+} can occur by PT-ET with prior protonation and reduction of Ru^{IV}=OH^{3+} in strongly acidic solutions. At higher pHs, with pH >> pK_a(Ru^{IV}=OH^{3+}), autocatalytic reduction of Ru^{IV}=O^{2+} to Ru^{III}-OH^{2+} occurs by partial reduction to Ru^{III}–O^+ followed by rapid protonation, further reduction to Ru^{II}-OH_2^{2+}, and cross-surface comproportionation, resulting in narrow, kinetically skewed voltammetric waves.

Water oxidation in non-aqueous environments

Water oxidation in Photosystem II occurs at the Oxygen Evolving Complex (OEC) which is embedded in the hydrophobic thylakoid membrane with water a limiting reagent. We have demonstrated catalytic water oxidation in nonaqueous solvents with water as a limiting reagent by, $Ru(Mebimpy)(bpy)(OH_2)^{2+}$ **1** in solution and $Ru(Mebimpy)(4,4'\text{-}(PO_3H_2CH_2)_2bpy)(OH_2)]^{2+}$ **1-PO_3H_2**, on the surfaces of conductive, planar FTO (fluoride-doped SnO_2) and nanoITO Figure 1.3. The rate of water oxidation in propylene carbonate (PC) or trifluoroethanol (TFE) with added water is enhanced by a factor of 300 compared to water as solvent and occurs by a pathway first order in H_2O.

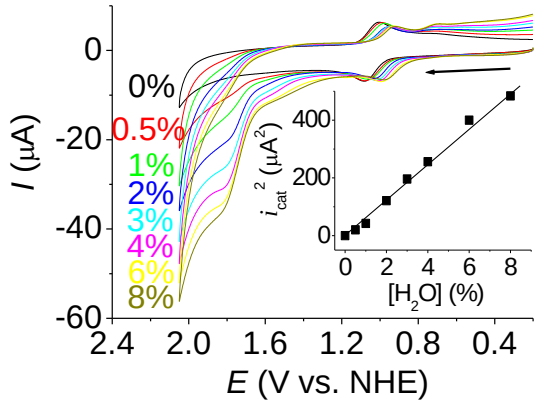

Figure 1.3. CVs of 1 mM 1 in 0.1 M $^{n}Bu_4NPF_6$/PC with addition of increasing amounts of water as indicated in the figure. The inset shows a plot of i_{cat}^2 (background subtracted) at 1.85 V (vs NHE) vs [H_2O], note eq 2. Electrode, GC; scan rate, 100 mV/s.

Water oxidation intermediates

Any mechanism for water oxidation near the thermodynamic potential for the H_2O/O_2 couple is necessarily complex due to the requirement for $4e^-/4H^+$ loss and O-O bond formation. Mechanistic complexity, however, creates an opportunity to examine intermediates that appear in the catalytic cycle for possible catalytic activity with alternate substrates.

Catalyst **1-PO_3H_2** was utilized for the electrocatalytic oxidation of the alkylaromatic hydrocarbons toluene, ethylbenzene, and cumene. Oxidation of hydrocarbons has a direct relation to fuel cell development and conversion of natural gas to liquid fuels. Since the hydrocarbons were not miscible with aqueous solutions, a new solvent system composed of propylene carbonate (PC) and 1 % water by volume with 0.1M $LiClO_4$ as electrolyte was constructed to carry out the oxidations. PC was chosen due to its oxidative stability and miscibility with water and hydrocarbons, and water was added to the system as a source of oxygen atoms in order to propagate the catalytic cycle. Cyclic voltammetry and steady state current measurements were able to determine that the catalytic rate constant for the oxidation of ethylbenzene was 2.5 ± 0.2 M^{-1} s^{-1}, which is comparable to the highest rate constants previously reported for hydrocarbon oxidations under similar conditions. Controlled potential electrolysis followed by product determination from mass spectroscopy showed that acetophenone was produced with a 95% Faradaic efficiency. The H/D kinetic isotope effect was determined by to be k_{C8H10}/k_{C8D10} = 1.2 ± 0.2 in PC/1% H_2O (I = 0.1 M $LiClO_4$, 23 ± 2 ^{o}C). The small magnitude of the KIE value is inconsistent with a mechanism involving hydride or hydrogen atom transfer (HAT) from ethylbenzene to the oxidant in the rate limiting step, however, direct O-atom insertion mechanisms with relatively small H/D KIE magnitudes have been reported.

A mechanism consistent with the experimental observations is shown in Scheme 1.2. The mechanism features rate limiting O-atom insertion into a C-H bond to give an intermediate with 1-phenylethanol in the coordination sphere (eq. 1.10a). Once formed, this $2e^-$ intermediate undergoes further $2e^-/2H^+$ oxidation to the coordinated ketone followed by hydrolysis. There is no evidence for buildup of the intermediate alcohol, 1-phenylethanol. Independent rate

measurements show that electrocatalytic oxidation of 1-phenylethanol occurs with $k_{cat} \approx 7.5\ M^{-1}\ s^{-1}$, or > 3x that of ethylbenzene catalysis, are consistent with oxidation of the alcohol in the coordination sphere of the intermediate in eq. 1.10b before it undergoes hydrolysis eq. 1.10c.

Scheme 1.2. Proposed oxygen-atom insertion mechanism for electrocatalytic ethylbenzene oxidation by *nano*ITO**|1-PO$_3$H$_2$**.

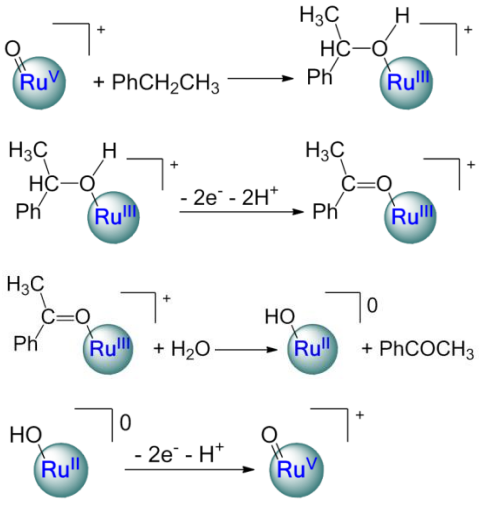

(1.10a)

(1.10b)

(1.10c)

(1.10d)

$$PhCH_2CH_3 + H_2O \xrightarrow{-4e^- - 4H^+} PhCOCH_3 \quad (1.11)$$

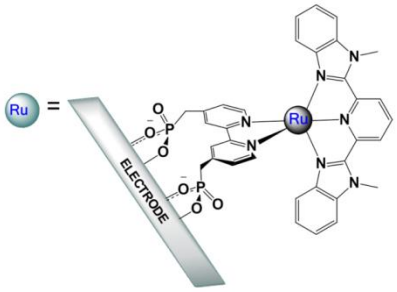

Water Oxidation from Cu salts

In another aspect, our work highlights a remarkable and previously unexpected research finding, that simple Cu(II) salts in concentrated bicarbonate/carbonate and phosphate buffer solutions act as rapid, efficient electrocatalysts for water oxidation. As showed in Figure 1.4, the roles of HCO_3^-/CO_3^{2-} or HPO_4^{2-}/PO_4^{3-} are essential in avoiding precipitation of $Cu(OH)_2$ ($K_{sp}(Cu(OH)_2) = 4.8 \times 10^{-20}$), $CuCO_3$ ($K_{sp}(CuCO_3) = 1.4 \times 10^{-10}$) or $Cu_3(PO_4)_2$ ($K_{sp}(Cu_3(PO_4)_2) = 1.40 \times 10^{-37}$) and in coordination stabilization of higher oxidation state Cu(III) and/or Cu(IV) intermediates. Water oxidation occurs by kinetically well-defined pathways either first or second order in [Cu(II)], depending on solution conditions with evidence for oxidized, presumably peroxide, intermediates. The rate of water oxidation in 1 M CO_3^{2-} is especially rapid and sustained for extensive periods. These results open new doors in the emerging science and

technology of "solar fuel" production and should be of interest broadly and of great potential for practical application.

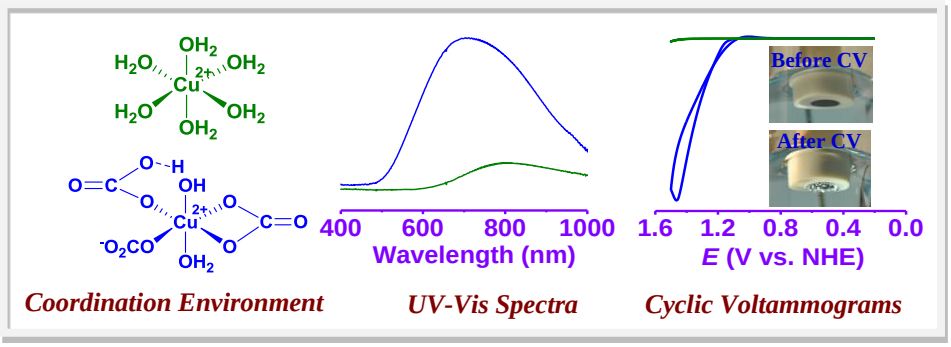

Figure 1.4. (Left) Proposals for the coordination environments of Cu(II) in water or $CO_2/HCO_3^-/CO_3^{2-}$ aqueous solution. (Middle) The corresponding UV-Vis spectra of 1 mM Cu(II) in water or in 1 M Na_2CO_3 (pH ~10.8). (Right) CVs in 1 M Na_2CO_3 (pH ~10.8) at a BDD electrode (0.071 cm^2) with and without of added 3 mM $CuSO_4$.

References:

(1) Hanson, K.; Torelli, D. A.; Vannucci, A. K.; Brennaman, M. K.; Luo, H.; Alibabaei, L.; Song, W.; Ashford, D. L.; Norris, M. R.; Glasson, C. R. K.; Concepcion, J. J.; Meyer, T. J. Self-Assembled Bilayer Films of Ruthenium(II)/Polypyridyl Complexes through Later-by-Layer Deposition on Nanostructured Metal Oxides. *Angew. Chem. Int. Ed.* **2012**, 51, 12782

(2) Chen, Z. F.; Meyer, T. J.* "Copper(II) catalysis of water oxidation." *Angewandte Chemie International Edition* **2013**, *52(2)*, 700-703.

2. Electrocatalytic Hydrogen Evolution

In previous reports, we have shown that complex **1**, note Figure 2.1, is a robust electrocatalyst toward CO_2 reduction in acetonitrile[1]. Here, we show that complex **1** is also a catalyst for water or proton reduction to hydrogen[2]. With water added to acetonitrile, the initial step is ligand-based reduction followed by proton abstraction from water to give the hydride, $[Ru^{II}(tpy)(bpy)(H)]^+$. The hydride is the active form of the catalyst toward H_2 evolution. Figure 2.2(a) shows CVs of Ar-deaerated solutions of **1** in 0.1 M $^nBu_4NPF_6/CH_3CN$ with increasing amounts of added water at a glassy carbon electrode and Figure 2.2(b) a series of CVs with 10% added water obtained at different negative switching potentials. Waves O1 and O2 in the insets arise from the re-oxidation of intermediates that form in the hydrogen evolution scheme.

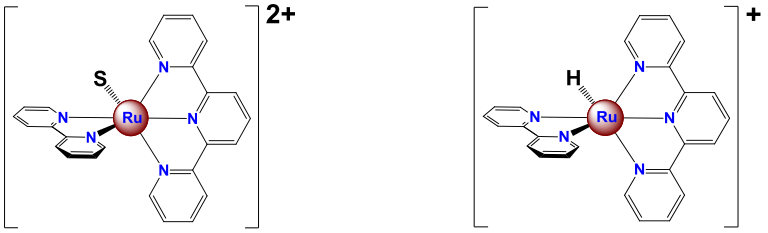

1 **2**

Figure 2.1. Structures of the polypyridyl Ru catalyst ($[Ru^{II}(tpy)(bpy)(S)]^{2+}$) **1** (S is solvent), and the Ru hydride ($[Ru^{II}(bpy)(bpy)(H)]^{+}$) **2**.

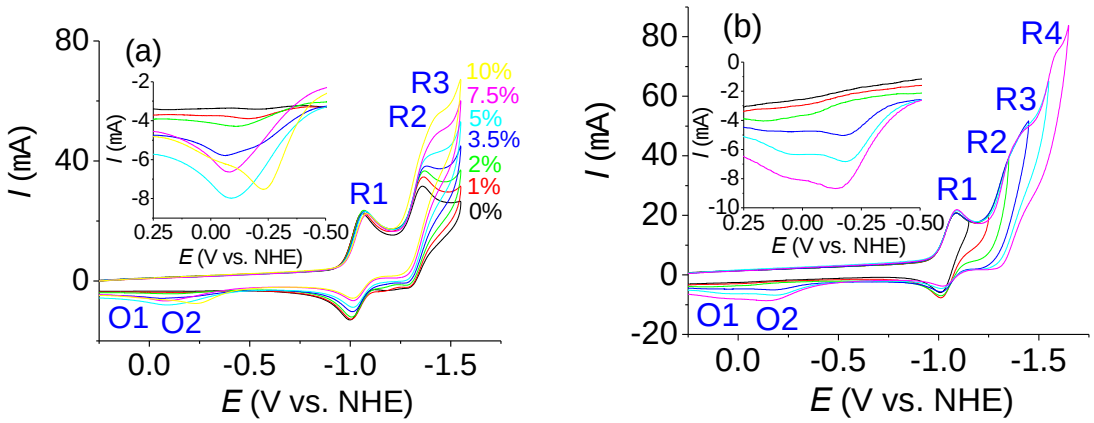

Figure 1.2. (a) Cyclic voltammograms of 1 mM **1** in 0.1 M $^{n}Bu_4NPF_6/CH_3CN$ under Ar with addition of increasing amounts of water (0–10% v:v; 0–5.5 M). (b) Cyclic voltammograms of 1 mM **1** in 10 % H_2O (v:v, 5.5 M), 0.1 M $^{n}Bu_4NPF_6/CH_3CN$ under Ar with reductive scans to increasingly negative potentials. The inset shows a magnified view of return, oxidative scans between −0.5 to 0.25 V following a reductive scan. Glassy carbon electrode; scan rate 100 mV/s.

The mechanism for electrocatalytic reduction of water and added weak acids to hydrogen is shown in Figure 2.3. As in CO_2 reduction, water reduction catalysis is initiated by reduction at the polypyridyl ligands. The *in situ* electrogenerated $[(tpy)(bpy)Ru^{II}(H)]^{+}$ is not sufficiently reactive to release hydrogen on the CV time scale with 10% added water. Hydrogen evolution is significantly promoted by tpy-based reduction to give $[(tpy^{-})(bpy)Ru^{II}(H)]^{0}$ at $E_{p,c}$ = –1.41 V (wave R3 in Figure 2.2b). It reacts with water in the rate limiting step with a H_2O/D_2O kinetic isotope effect (KIE) of 3.7 to give an additional intermediate, presumably the dihydrogen complex, $[(tpy)(bpy)Ru(H_2)]^{+}$, eq 2.1. The intermediate undergoes a characteristic reduction at $E_{p,c}$ = –1.55 V (wave R4). The catalytic cycle is completed by loss of hydrogen, solvolysis, and re-entry into the catalytic cycle.

$$[(tpy^{-})(bpy)Ru^{II}(H)]^{0} + H_2O \rightarrow [(tpy)(bpy)Ru(H_2)]^{+} + OH^{-} \qquad (2.1)$$

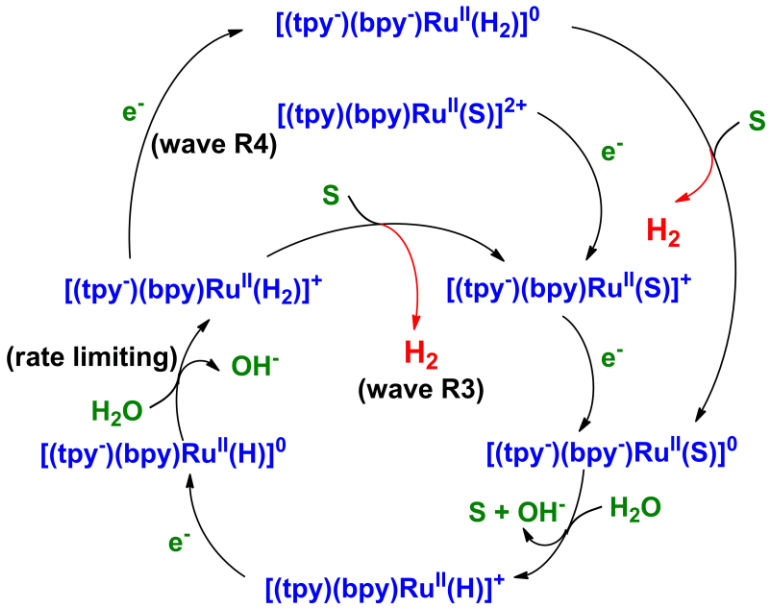

Figure 2.3. Proposed mechanism for electrocatalytic reduction of water by **1** (S = CH_3CN).

A considerable rate enhancement for hydrogen evolution by **1** was observed with added weak acids, qualitatively, with the extent of rate enhancement scaling with the strength of the acid and its pK_a. A series of CVs with added [^{n}Bu$_4$N][H_2PO_4] (pK_a = 7.2 in water compared to pK_a = 15.7 for water in water) is shown in Figure 2.4. With > 10 mM added $H_2PO_4^-$, significant rate enhancements for hydrogen evolution are observed, by a factor of 10^4 fold compared to water. Under these conditions, there is no evidence for re-oxidation of [(tpy)(bpy)Ru^{II}(H)]$^+$ at wave O1 or of the dihydrogen intermediate at wave O2. These observations point to hydrogen evolution with added $H_2PO_4^-$ by a second catalytic cycle, Figure 2.5. In this cycle, the rate limiting step is formation of the hydride following a second reduction at bpy. Once the hydride is formed, it undergoes a rapid reaction with $H_2PO_4^-$ to give hydrogen and the solvent-coordinated complex which re-enters the catalytic cycle.

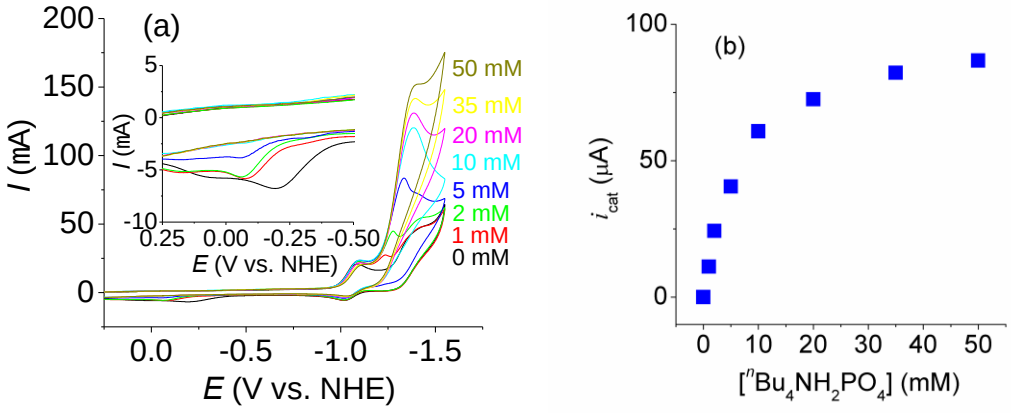

Figure 2.4. (a) Cyclic voltammograms of 1 mM **1** in 10% H_2O, 0.1 M ^{n}Bu$_4$NPF_6/CH_3CN under Ar with addition of increasing amounts of [^{n}Bu$_4$N][H_2PO_4]. The inset shows a magnified view of return, oxidative scans between −0.5 to 0.25 V following a reductive scan. Glassy carbon

electrode: scan rate, 100mV/s. (b) Plot of catalytic currents during electrolysis at −1.38 V, i_{cat} (background subtracted), *vs.* concentration of added $H_2PO_4^-$.

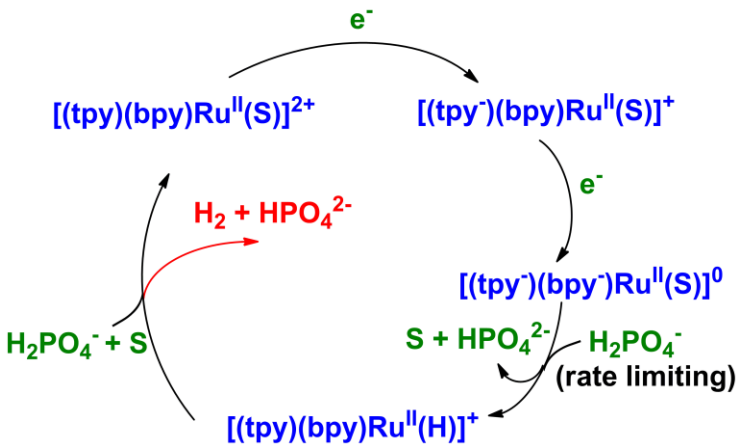

Figure 2.5. Proposed mechanism for electrocatalytic reduction of $H_2PO_4^-$ by **1** (S = CH_3CN).

Hydrogen evolution also occurs with other added weak acids, *e.g.* [^{n}Bu$_4$N][HCO_3] (pK_a ~10.3 in water) where there is evidence for both [Ru(tpy)(bpy)(H)]$^+$ and its reduced form as intermediates. Similar results were obtained for [Ru(tpy)(bpy)Cl]$^+$, following its reduction, solvolysis, and conversion to the hydride, and for other structurally related polypyridyl ruthenium complexes.

In the catalytic cycle in Figure 2.3, enhanced hydride donor reactivity of the hydride is induced by the electron reservoir effect and activation of the hydride by ligand-based reduction. As noted above, Creutz, *et al*., had demonstrated an extensive hydride reactivity of [Ru(tpy)(bpy)(H)]$^+$ toward a number of hydride acceptors, CO_2, formaldhyde, *etc*. We extended this reactivity to the reduction of organic functional groups, in particular, to the reduction of acetone to *iso*-propanol. In 10% H_2O/CH_3CN under Ar, no significant reaction is detected between [Ru(tpy)(bpy)(H)]$^+$ and acetone after 12 h. However, upon *in situ* electrochemical reduction, [Ru(tpy$^-$)(bpy)(H)]^0 is an active electrocatalyst toward reduction of acetone to *iso*-propanol in competition with hydrogen production.

Syngas Production

The electrochemical investigations on CO_2 and water reduction revealed well-defined mechanisms based on common intermediates. In these reactions electrocatalytic reduction of H_2O or CO_2 by [Ru^{II}(tpy)(bpy)($NCCH_3$)]$^{2+}$ is initiated by ligand-based reduction which activates the metal toward displacement of bound CH_3CN by CO_2 in the dry solvent or, with added water, by proton abstraction from H_2O to give the hydride, [Ru^{II}(tpy)(bpy)(H)]$^+$. In dry CH_3CN, ligand-based reduction of [Ru^{II}(tpy)(bpy)($NCCH_3$)]$^{2+}$ induces coordination of CO_2 to give the metallocarboxylate, [Ru^{II}(tpy)(bpy)(CO_2^{2-})]^0 which undergoes further reduction and O^{2-} loss to CO_2 to give the corresponding CO complex. With added weak acids – $H_2PO_4^-$, HCO_3^- – the hydride protonates to give a dihydrogen intermediate, liberating H_2.

In solutions saturated in CO_2 with 10% H_2O and added weak acid $H_2PO_4^-$, we found a competition exists between the H_2 evolution and CO_2 reduction pathways[3]. In current

experiments, we have shown that electrocatalytic reduction under these conditions gives syngas mixtures of H_2 and CO with the ratio dictated by the relative amount of acid added. Given the importance of syngas mixtures as precursors to methanol and other hydrocarbons this is an important observation in demonstrating use of a single catalyst to carry out this important reaction with important implications for potential electrocatalytic and photoelectrocatalytic approaches to syngas production.

CO_2 splitting

In spite of formidable challenges in chemical reactivities for both water oxidation and CO_2 reduction, we illustrated that the transition metal complex $[(tpy)(Mebim\text{-}py)Ru^{II}(S)]^{2+}$ (tpy = 2,2':6',2''-terpyridine; Mebim-py = 3-methyl-1-pyridylbenzimidazol-2-ylidene; S = solvent) is a robust, reactive electrocatalyst both for water oxidation to O_2 in aqueous solution and for CO_2 reduction to CO in acetonitrile with the single catalyst applied to CO_2 splitting into CO and O_2 in a two-compartment electrochemical cell, as showed in Figures 2.6 and 2.7. In its simplicity, the contrast of the setup in Figure 2.6 with natural photosynthesis is striking. Photosynthesis in green plants involves thousands of atoms, five membrane-bound integrated assemblies, and the Calvin cycle and evolved over billions of years to achieve CO_2 splitting into oxygen and carbohydrates. In the electrochemical/photoelectrochemical approach, single catalysts or pairs of catalysts are combined with semiconductors, electrodes, wires, and membranes to connect the half reactions and exchange electrons and protons.

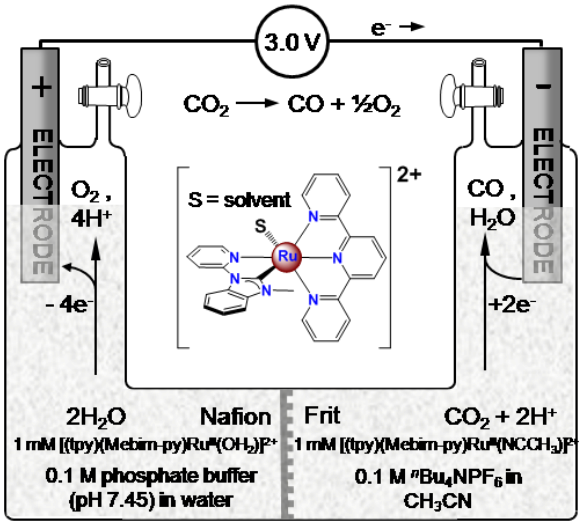

Figure 2.6 Schematic diagram for the two-compartment, Nafion|Frit-separated electrochemical cell for CO_2 splitting.

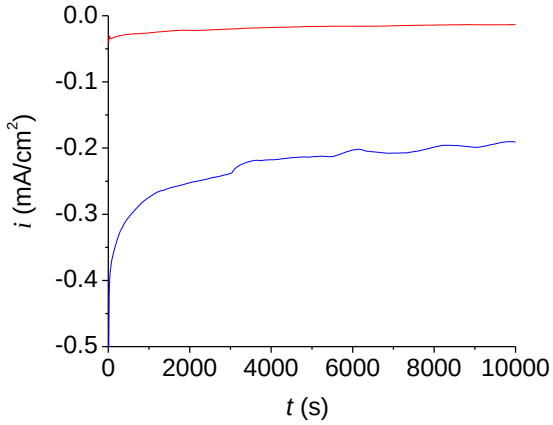

Figure 2.7. Blue line: As in Figure 2.6, controlled potential electrolysis at 3.0 V at two boron doped diamond electrodes (~0.85 cm^2). Red line: background current without added catalyst.

Although the above study was the first example of a single molecule catalyst for CO_2 splitting to the best of our knowledge, long term performance was limited by slow solvent inter-permeability across the membrane separator, slow carbene ligand oxidation at the anode, and catalyst precipitation at the cathode. As an extension of our Cu(II) catalysis of water oxidation, together with our interest in CO_2 splitting by single catalysts, we report here that, under appropriate solution conditions, simple Cu(II) salts are reactive as water oxidation electrocatalysts and its reduction form, Cu(0) film formed by electroplating from Cu(II) capable of CO_2 reduction in electrolysis cell of two compartments. The two half reactions provide a basis for net electrochemical and solar splitting of CO_2 into $CO/HCOO^-$ and O_2, as showed in Figure 2.8.

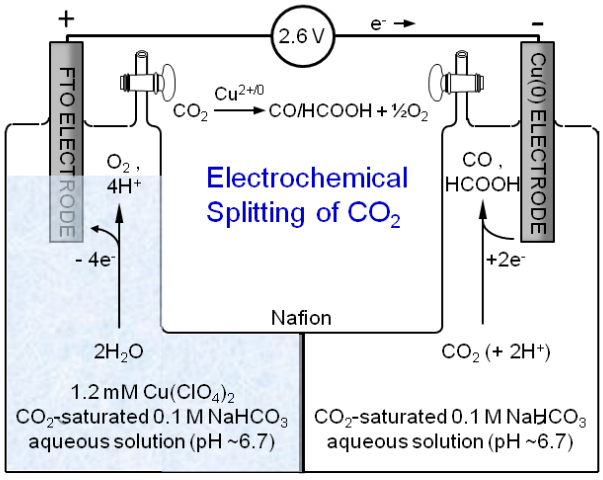

Figure 2.8. Schematic diagram for a two-compartment, two-electrode Nafion-separated electrochemical cell for CO_2 splitting by simple Cu(II) in CO_2-saturated 0.1 M $NaHCO_3$ aqueous solution (pH ~6.7).

References:

(1) Chen, Z. F.; Chen, C. C.; Weinberg, D. R.; Kang, P.; Concepcion, J. J.; Harrison, D. P.; Brookhart, M. S.; Meyer, T. J. Electrocatalytic reduction of CO2 to CO by polypyridyl ruthenium complexes. *Chem. Comm.* **2011**, 47, 12607-12609.

(2) Chen, Z. F.; Glasson, C. R. K.; Holland, P. L.; Meyer, T. J. Electrogenerated polypyridyl ruthenium hydride and ligand activation for water reduction to hydrogen and acetone to iso propanol. *Phys. Chem. Chem. Phys.* **2013**, 15(24), 9503-9507.

(3) Chen, Z. F.; Concepcion, J. J.; Brennaman, M. K.; Kang, P.; Norris, M. R.; Hoertz, P. G.; Meyer, T. J.* "Splitting CO_2 into CO and O_2 by a single catalyst." *Proceedings of the National Academy of Sciences, USA* **2012**, *109(39)*, 15606-15611.

(4) Chen, Z. F.; Kang, P.; Zhang, M. T.; Stoner, B. R.; Meyer, T. J.* "Cu(II)/Cu(0) electrocatalyzed CO_2 and H_2O splitting." *Energy & Environmental Science* **2013**, *6*, 813-817.

3. <u>H_2 Production in Dye Sensitized Photoelectrosynthesis Cell(DSPEC): Interfacial Dynamics and Efficiencies</u>

We explored Dye Sensitized-Photoelectrochemical Cell (DSPEC) configurations for important photochemical reactions such as water splitting, $2\ H_2O + 4\ h\nu \rightarrow O_2 + 2\ H_2$, and organic dehydrogenation/oxidation, e.g., $RR'CHOH + 2\ h\nu \rightarrow RR'C{=}O + H_2$ with visible light. This approach follows from the Dye Sensitized Solar Cells (DSSC) pioneered by Gratzel and coworkers. In our studies we focused on the relationship between interfacial photophysical dynamics and hydrogen production efficiencies in DSPEC.

Charge separation and recombination dynamics (eq 3.1 and figure 3.1) have been investigated in DSPEC cells with $Ru^{II}(bpy)_2(4,4'\text{-}((HO)_2OP)_2bpy)]^{2+}$ attached to FTO|TiO_2 substrates (**TiO_2-RuP**). Phosphonates are appealing compared to commonly used carboxyates functional group because of enhanced surface stability in aqueous media.

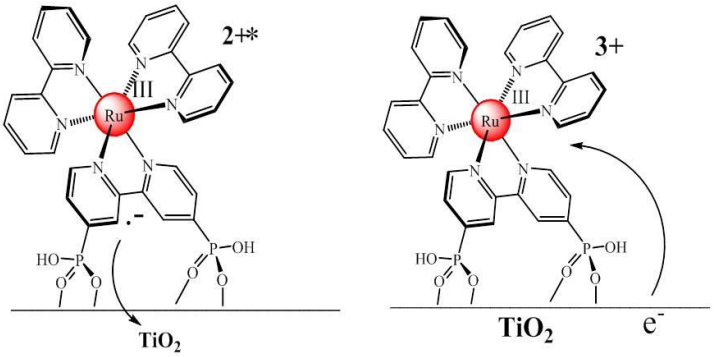

Figure 3.1. Interfacial electron-transfer dynamics and hydrogen formation at TiO2-RuP photoanode

$$TiO_2\text{-}Ru^{II} + h\upsilon \rightarrow TiO_2\text{-}Ru^{II}* \rightarrow TiO_2(e^-)\text{-}Ru^{III} \rightarrow TiO_2\text{-}Ru^{II} \quad (3.1)$$

We have shown that the electron injection yield from **RuP** excited states to TiO_2 is favored by low pH, but back electron transfer kinetics is also enhanced in acidic media. In addition, back electron transfer can be tuned by applying external bias or reducing light intensity (Figure 3.2). These effects originate from combination of effects: (i) pH dependence of TiO_2 conduction band/trap states (E = -0.16 -0.059pH vs NHE); (ii) injected electron density in TiO_2; (iii) the quasi-Fermi level of TiO_2

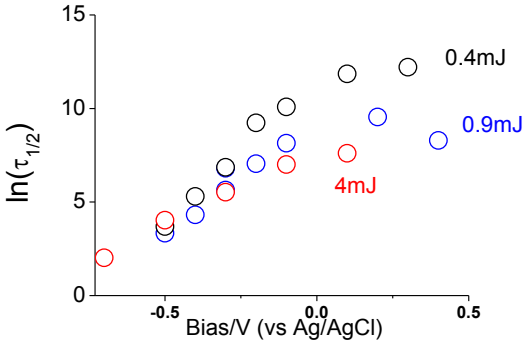

Figure 3.2. Half lifetime of photogenerated TiO_2-$Ru^{III}P$ at pH 1 in aqueous solution under various external bias and excitation intensities

We have investigated photoelectrochemical hydrogen generation in a DSPEC cell based on eq 1 with the photogenerated holes, as TiO_2-Ru^{III}, reduced by external donors, triethanolamine (TEOA) or ethylenediaminetetraacetate (EDTA) to provide reductive equivalentsto a second, counter electrode for proton reduction to hydrogen, eq. 3.2 and 3.3. We explored this phenomenon by transient absorption (TA), transient photocurrent, photon-to-current conversion efficiency (IPCE) measurements, and by hydrogen production under steady state light illumination.

$$Pt \| TiO_2(e^-)\text{-}Ru^{III} + D \rightarrow Pt \| TiO_2(e^-)\text{-}Ru^{II} + D_{ox} \rightarrow Pt(e) \| TiO_2\text{-}Ru^{II} + D_{ox} \quad (3.2)$$

$$H^+ + Pt(e) \rightarrow \tfrac{1}{2} H_2 \quad (3.3)$$

The reaction of TEOA and EDTA was monitored by transient absorption (TA). The observed rate constant for RuP regeneration reached a plateau at ~ 10mM of TEOA at pH 6.7 (Figure 3.3A). The reduction of $Ru^{III}P$ by EDTA was more efficient (Figure 3.3B) due to its higher affinity to semiconductor surface, as well as a better pre-association with surface bond, photo-generated $Ru^{III}P$. In the presence of external donors, electron collection efficiencies were obtained by transient photocurrent measurements, as a function of applied potential (Figure 3.4A), with back electron transfer dynamics monitored simultaneously (Figure 3.4B). The conduction band potential of TiO_2 was slightly lower than potential of H^+/H_2 redox couple, therefore an positive bias was necessary for efficient proton reduction at the Pt counter electrode. Sufficient positive bias decreases the rate of back electron transfer to surface $Ru^{III}P$ and facilitates electron transport through TiO_2 film to external circuit. The interfacial dynamics data revealed optimized condition for long-lived charge separated states for hydrogen production. DSPEC performance (incident photon to current conversion, IPCE) under steady state light irradiation (Figure 3.5) agreed well with results obtained by transient measurements.

The with quantum yields for hydrogen generation approached 15% in DSPEC with 0.2 V bias in the presence of EDTA as electron donor.

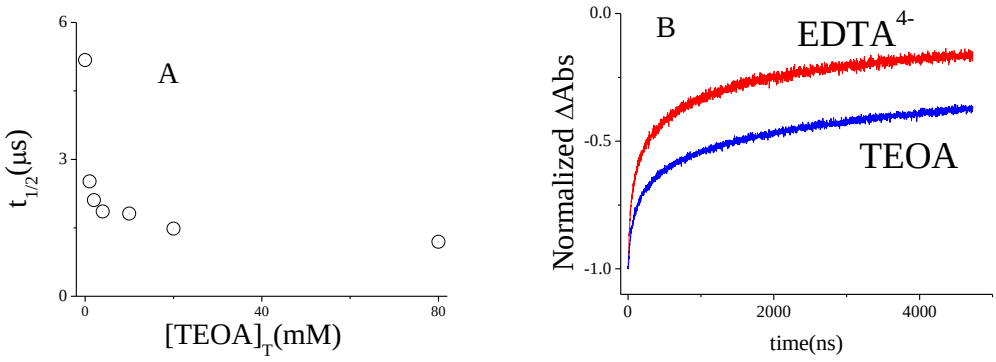

Figure 3.3. (A) Half lifetime ($t_{1/2}$) for Ru(III) following laser flash excitation in the presence of different concentration of TEOA. (B) Regeneration of TiO_2-$Ru^{II}P$ monitored by 450nm transient absorption in the presence of 80 mM TEOA and 20 mM EDTA under open circuit condition.

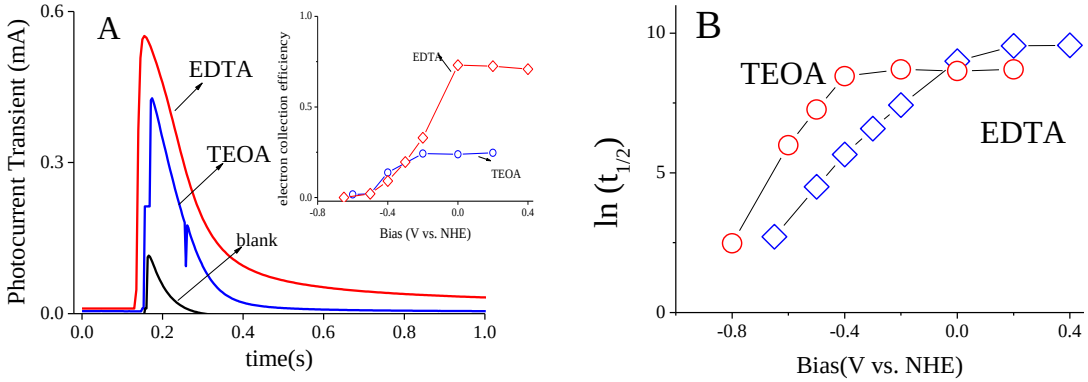

Figure 3.4. (A) Transient photocurrent induced by one laser pulse with TEOA or EDTA as electron donor in DSPEC with 0.2V bias vs. NHE. Insert, electron collection efficiency at different applying bias in the presence of both donors; (B) Plot of ln($t_{1/2}$,μsec) vs applied bias for TiO2(e)-$Ru^{III}P$ with added TEOA (o), pH 6.7, and $EDTA^{4-}$ (◊), pH 4.5.

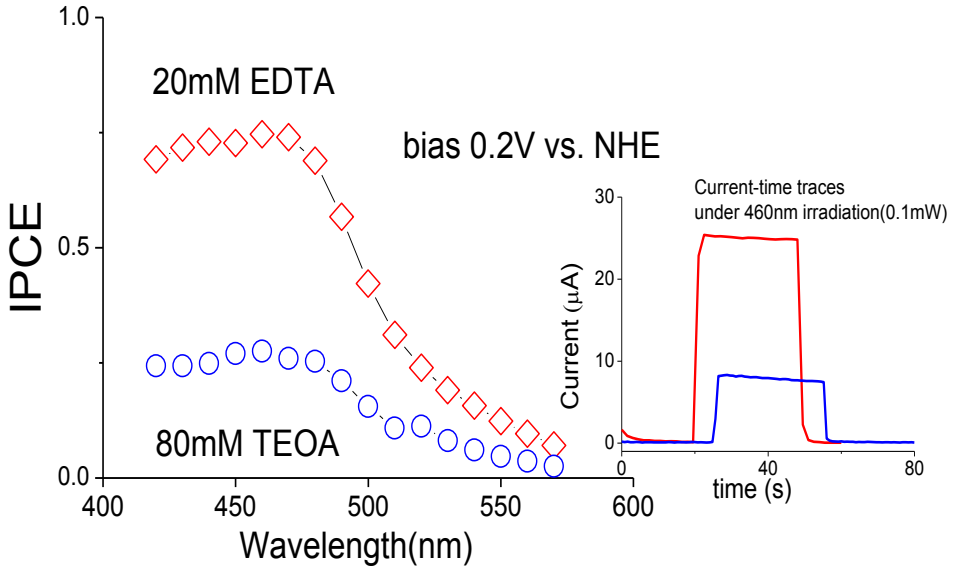

Figure 3.5. Incident photon to current efficiency (IPCE) for DSPEC with 0.2 V bias with TEOA or EDTA as electron donor.

Photo-Induced Multiple oxidative Equivalent Accumulation/Catalyst Activation of Chromophore-Catalyst Assembly Ru_a-Ru_b-OH_2 on TiO_2

A major challenge for water splitting, photochemical oxidation of organics, or CO2 reduction in DSPEC cells exists due to the multi-proton/and multi-electron nature of the reactions. This requires multiple photon events, all of which are in competition with back electron transfer, to build up the required multiple redox equivalents. We are investigating a series of ruthenium polypyridyl assemblies which combine light harvesting and electron injection in TiO2 with delivery of oxidative equivalents to a remote catalyst for water/organic oxidation (eq 3.4 – 3.6).

$$TiO_2\text{-}Ru_a^{II}\text{-}Ru_b^{II}OH_2 \xrightarrow{h\nu} TiO_2\text{-}Ru_a^{II*}\text{-}Ru_b^{II}OH_2 \xrightarrow[\text{injection}]{\text{electron}} TiO_2(e^-)\text{-}Ru_a^{III}\text{-}Ru_b^{II}OH_2$$

$$\xrightarrow[-H^+]{\text{electron transfer}} TiO_2(e^-)\text{-}Ru_a^{II}\text{-}Ru_b^{III}OH \qquad (4)$$

$$TiO_2\text{-}Ru_a^{II}\text{-}Ru_b^{III}OH \xrightarrow{h\nu} TiO_2\text{-}Ru_a^{II*}\text{-}Ru_b^{III}OH \xrightarrow[\text{injection}]{\text{electron}} TiO_2(e^-)\text{-}Ru_a^{III}\text{-}Ru_b^{III}OH$$

$$\xrightarrow[-H^+]{\text{electron transfer}} TiO_2(e^-)\text{-}Ru_a^{II}\text{-}Ru_b^{IV}O \qquad (5)$$

$$TiO_2\text{-}Ru_a^{II}\text{-}Ru_b^{IV}O \xrightarrow{h\nu} TiO_2(e^-)\text{-}Ru_a^{III}\text{-}Ru_b^{IV}O \xrightarrow{\text{electron transfer}} TiO_2(e^-)\text{-}Ru_a^{II}\text{-}Ru_b^{III}OOH$$

$$\xrightarrow{h\nu} TiO_2(2e^-)\text{-}Ru_a^{II}\text{-}Ru_b^{IV}OOH \xrightarrow{H_2O} TiO_2\text{-}Ru_a^{II}\text{-}Ru_b^{II}OH_2 + O_2 + H^+ \qquad (6)$$

We have developed several chromophore catalyst assemblies with carboxylic or phosphonate functional group (Figure 3.6, 1C and 1P). In these molecular assemblies, Ru_a^{II}-$Ru_b^{III}OH$ and Ru_a^{II}-$Ru_b^{IV}O$ could be generated electrochemically on high surface area conducting In2O3 electrode, which provided spectral information for different oxidizing/activated states (Figure 3.7). The photoinduced generation of $TiO_2(e^-)$-Ru_a^{II}-Ru_b^{III} and $TiO_2(e^-)$-Ru_a^{II}-Ru_b^{IV} were confirmed by transient absorption measurements (Figure 3.8).

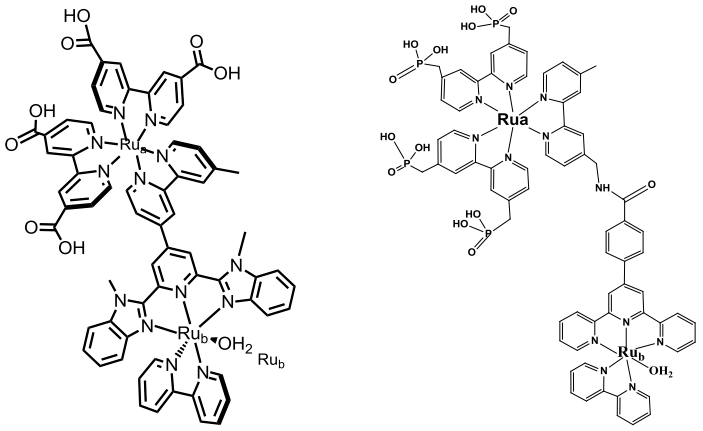

1C **1P**

Figure 3.6. Structures of the assemblies

Compared to chromphore RuP, 1C has much lower injection efficiency (~ 20%) due to competition between injection and excited decay from the remote catalysts site. Injection efficiency was improved for molecular assembly 1P, which has non-conjugated bridging ligand between chromophore and catalyst. Rates of back electron transfer in these molecular assemblies were greatly decreased, compared to monomeric analogs (Table 1). It is worth noting that for 1P, the lifetime of photogenerated TiO2(e^-)-$Ru^{II}Ru^{III}OH$ was extended to millisecond in pH 4.5 aqueous solution (Figure 3.9), which is a favored condition for light driven catalytic water oxidation.

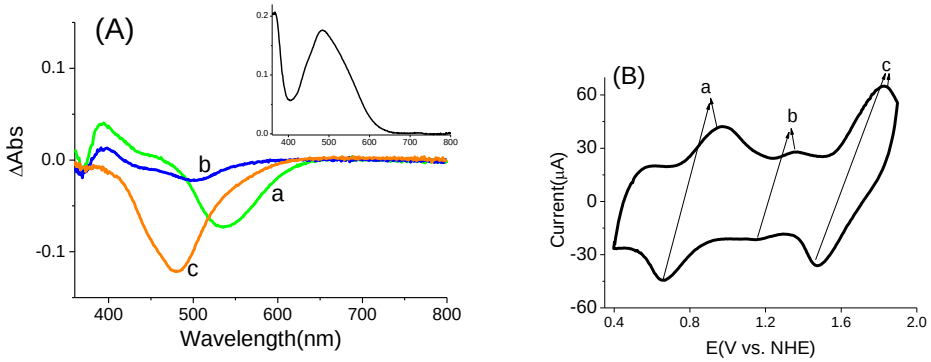

Figure 3.7. (A) Visible spectral changes accompanying reversible oxidation of *nano*ITO-Ru_a^{II}-$Ru_b^{II}OH_2$ to *nano*ITO-Ru_a^{II}-$Ru_b^{III}OH$ (**a**), to *nano*ITO-Ru_a^{II}-Ru_b^{IV}=O (**b**) and to *nano*ITO-Ru_a^{III}-

Ru_b^{IV}=O (**c**). Insert: spectrum of *nano*ITO-Ru_a^{II}-Ru_b^{II}-OH_2^{2+}. **(B)** Cyclic voltammogram of **1C** on *nano*ITO (10 mV/s).

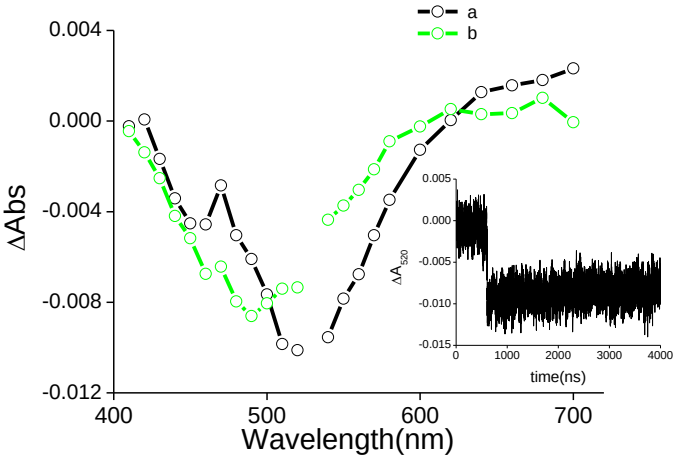

Figure 3.8. Transient absorption difference spectra obtained following 532 nm excitation of TiO_2-Ru_a^{II}-$Ru_b^{II}OH_2$ (**a**) and TiO_2-Ru_a^{II}-$Ru_b^{III}OH$ (**b)** in propylene carbonate with 2% Insert: Plot of transient absorbance-time trace monitored at 520 nm.

Table 3.1. Back electron transfer dynamics obtained from stretched exponential fit ($\Delta OD = Ae^{-(t/\tau)^{\beta}}$) for molecular assembly 1P, monomeric control chromophore and contral catalyst on TiO_2

Complex	Back Electron Transfer[b]	
	τ (μs)	β
1P	6.7	0.25
chromophore	1.8	0.29
catalyst	2.2	0.22

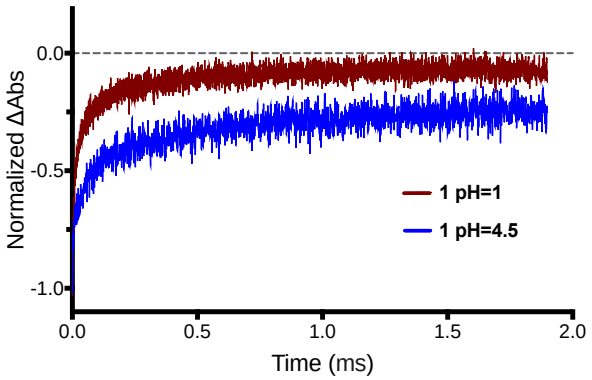

Figure 3.9. Absorbance-time traces for **1P** on TiO_2 following 532 nm laser flash (5.0 mJ) excitation with monitoring at 480 nm in 0.1 M $HClO_4$ (red) and at pH = 4.5 (0.18M $LiClO_4$ with 20mM NaOAc/HOAc buffer, blue).

Lithium intercalation dynamics at photoanode interfaces and effect of Lithium doping on dye sensitized photoelectrochemical cells (DSPECs)

Solar fuels production in dye sensitized photoelectrosynthesis cells (DSPEC) is a promising approach to solar energy conversion. The efficiency of DSPECs is highly dependent on small cations present at photoelectrode interfaces or doped into the semiconductor bulk, due to their impacts on the dynamics of photo-induced charge separation, recombination, and carrier transport at photoelectrode–electrolyte interfaces.

In our study, the dynamics of Li^+ diffusion at photoelectrodes/electrolyte interface was monitored *in situ* in a working DSPEC for hydrogen generation. The photoaonde was TiO2 mesoscopic film sensitized with [Ru(bpy)2(4,4'-PO(OH)2bpy)]2+ (**RuP**). As shown in **Figure 3.10**, **RuP** on TiO_2 was shown to be sensitive to the microscopic environments including external electric field (by electron injection into TiO_2) and local concentration of small cations including Li^+ and proton. Such spectral response of RuP was attributed to the change in metal to ligand charge transfer transition energy in the electric field (Stark effect), and the screening of electric field by cations. The spectral response provides simple method to time-resolve the cation diffusion dynamics.

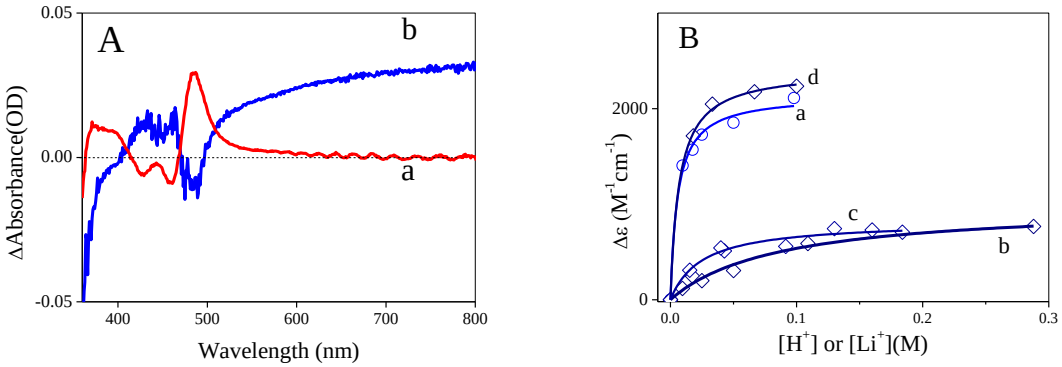

Figure 3.10. (A) Spectral change of TiO_2-RuP in electrolyte with/without 0.1 M Li^+ (a, red), and after applying a -0.7 V bias vs. NHE to the electrode for ~30 s ((b, blue); (B) Change in molar absorptivity of TiO_2-**RuP** at (482 ± 2) nm immersed in solutions with different concentrations of proton or Li^+: (a) proton in aqueous solution; (b) Li^+ in aqueous solution; (c) Li^+ in propylene carbonate (PC) with 5% water; (d) Li^+ in PC. The solid curves are fit from Langmuir isotherm equation

In DSPECs for hydrogen production, sacrificial electron donors, such as EDTA were used to regenerat $Ru^{III}P$ after electron injection. The reactions at the photoanode are summarized in eqn (3.7)–(3.10), where M^+ is the cation in the electrolyte and D is the electron donor. Eq (3.9) and (3.10) demonstrate the charge compensation at TiO_2 surface, i.e., cation intercalation/re-release, *coupled* to electron injection, recombination and transport at the interfaces.

TiO_2-$Ru^{II}P$ + hν → $TiO_2(e^-)$-$Ru^{III}P$ (3.7)

$TiO_2(e^-)$-$Ru^{III}P$ + D → $TiO_2(e^-)$-$Ru^{II}P$ + D^+ (3.8)

$TiO_2(e^-)$-$Ru^{II}P$ + M^+ → $TiO_2(e^-)$-$Ru^{II}P/M^+$ (3.9)

$TiO_2(e^-)$-$Ru^{II}P/M^+$ + electrolyte or FTO → TiO_2-$Ru^{II}P$ + M^+ (3.10)

The cation intercalation, triggered by electron injection was confirmed by spectral change of TiO_2-**RuP** photoanode (consistent with Figure 3.1 A, a), in DSPEC under both open circuit condition, where injected electrons accumulated in TiO2 conduction band/trap states(Figure 3.11), and with applied bias to extract electrons to external circuit (Figure 3.12). In addition, upon electron recombination, the intercalated Li^+ diffuse back to electrolyte bulk. The apparent rate for intercalation was much faster than re-release under the DSPEC operating condition, with both rate constants strongly solvents dependent (water >propylene carbonate–water mixture > propylene carbonate (**Table 3.2**).

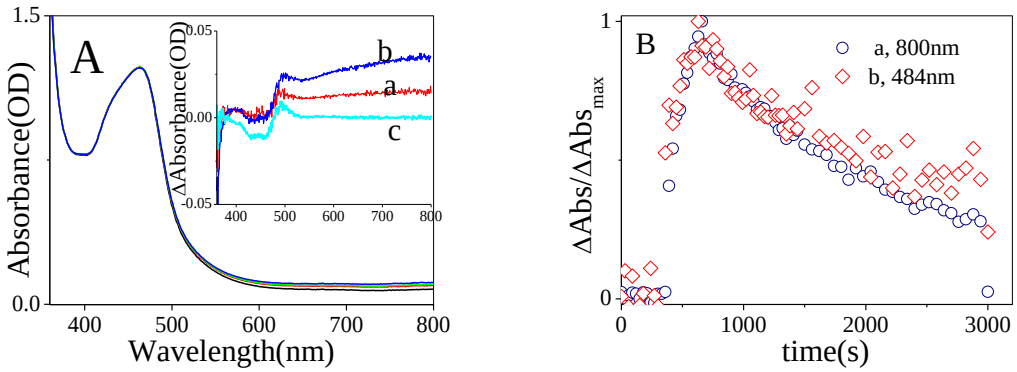

Figure 3.11. (A) Absorbance changes for TiO_2-**RuP** in a DSPEC under open circuit conditions. The electrolyte was 0.2 M $LiClO_4$ with 20 mM added $EDTA^{4-}$ at pH 4.5. light source was 445 nm LED (7.2 mW). Insert: Absorbance difference spectra relative to initial spectrum following (a) 30 s, (b) 280 s photolysis periods and (c) after complete discharge of the original electrode. (B) Rhe ratio of the absorption change to the maximum absorption changes at (a) 800 nm and (b) 489 nm extracted from the data in panel A.

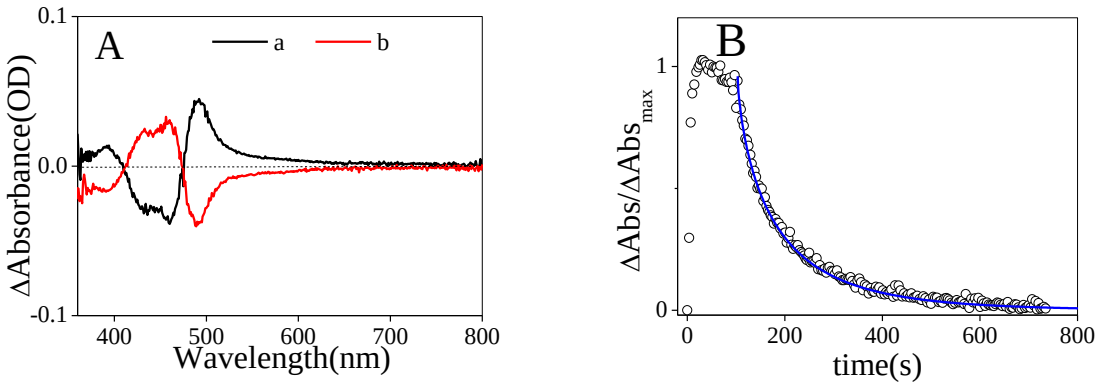

Figure 3.12. (A) Absorbance spectral changes for TiO_2-**RuP** in a DSPEC with 0.2 V applied bias vs. NHE: (a, black) difference between 120 s irradiation and before irradiation; (b, red) difference between 300 s and 10 s after the light was switched off. Light intensity at 445 nm was 7.2 mW. (B) Absorption-time change monitored at 489 nm under the same conditions as (A). The solid blue line on top is the stretched exponential fit to the decay data.

Table 3.2. Dynamics of Li^+ intercalation and release.

Electrolyte	Donor	$t_{1/2}$ for intercalation (sec)	$t_{1/2}$ for release(sec)
Water, pH 4.5	EDTA	5.5	50
PC	4-methoxy thioanisole	71	>5000
PC/5% water	4-methoxy thioanisole	70	1740

Our results clearly show that lithium diffusion back dynamics are much slower than electron transport/recombination. The difference in intercalation/release dynamics resulted Li^+ enrichment or doping in TiO_2 during DSPEC operation. This was supported by the change in the positive shift of TiO_2 conduction band/trap states, as shown in the cyclic voltammetry of TiO_2-RuP (**Figure 3.13**, a positive shift in the onset of the capacitive potential), as well as the increase in TiO2 electron lifetime. Our results provided a mechanistic insight of the change in DSSC or DSPEC efficiency during long term operation which was observed in other research groups. The photodriven cation doping provides an alternative means for controlling DSPEC efficiencies.

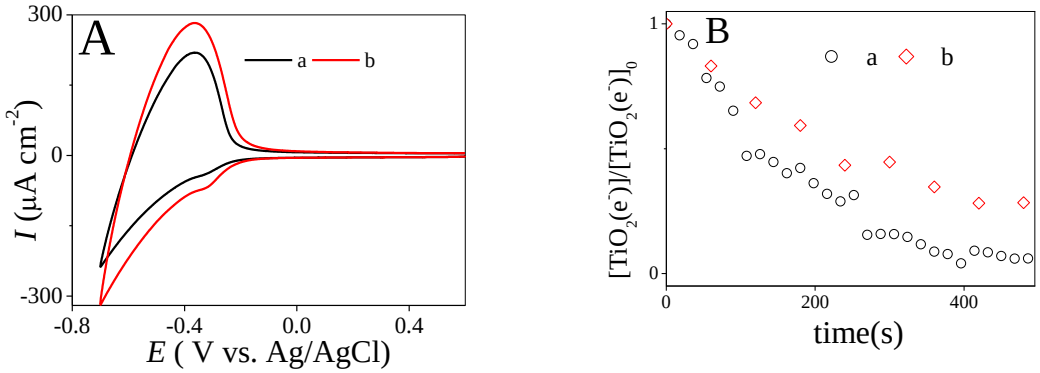

Figure 3.13. (A) Cyclic voltammograms of TiO_2-**RuP** (a) before and (b) after photolysis at open circuit for 30 min (445 nm, 7.2 mW) (B) $TiO_2(e^-)$ density change with time in the dark after 300 s photolysis at open circuit: (a) 1st run (b) 5th run. The electrolyte was 0.2 M $LiClO_4$ with 20 mM EDTA, pH 4.5. Scan rate: 0.1V s^{-1}

References:

(1) Song, W.; Luo, H.; Hanson, K.; Concepcion, J. J.; Brennaman, M. K.; Meyer, T. J. *Energy & Environmental Science* **2013**, *6*, 1240.

(2) Song, W.; Chen, Z.; Glasson, C. R. K.; Hanson, K.; Luo, H.; Norris, M. R.; Ashford, D. L.; Concepcion, J. J.; Brennaman, M. K.; Meyer, T. J. *Chemphyschem* **2012**, *13*, 2882.

(3) Glasson, C. R. K.; Song, W.; Ashford, D. L.; Vannucci, A.; Chen, Z.; Concepcion, J. J.; Holland, P. L.; Meyer, T. J. *Inorganic Chemistry* **2012**, *51*, 8637.

(4) Ashford, D. L.; Song, W.; Concepcion, J. J.; Glasson, C. R. K.; Brennaman, M. K.; Norris, M. R.; Fang, Z.; Templeton, J. L.; Meyer, T. J. *Journal of the American Chemical Society* **2012**, *134*, 19189.

(5) Song, W.; Glasson, C. R. K.; Luo, H.; Hanson, K.; Brennaman, M. K.; Concepcion, J. J.; Meyer, T. J. *Journal of Physical Chemistry Letters* **2011**, *2*, 1808.

(6) Song, W.; Brennaman, M. K.; Concepcion, J. J.; Jurss, J. W.; Hoertz, P. C.; Luo, H.; Chen, C.; Hanson, K.; Meyer, T. J. *Journal of Physical Chemistry C* **2011**, *115*, 7081.

4. Layer-by-Layer Synthesis of a Porphyrin and Ru(II) Water Oxidation Catalyst Assembly on Nanostructured Metal Oxides

Dye-sensitized solar cells (DSSC) and photoelectrosynthesis cells (DSPEC) provide viable strategies for solar-to-electricity or fuel using sunlight. In both a key is excitation and injection by surface-bound chromophores or chromophore-catalyst assemblies on nanostructured metal oxide surfaces. Organic chromophores are desirable in such applications given their potentially low cost, high light absorptivity, and ability to be modified systematically by chemical synthesis. Porphyrins with high light absorptivities in the visible are an advantageous choice in terms of

spectral coverage and energetic. Although reasonably large numbers of porphyrin have been studied for DSSC applications, there are few examples for DSPEC application.

In this report we describe the synthesis of an electron deficient porphyrin with phosphonate anchors and construction of chromophore-catalyst bilayer assemblies on nanostructured metal oxides by a layer-by-layer approach pioneered earlier for polypyridyl complexes of Ru. Relevant structures are shown in Figure 4.1. The free base porphyrin shown has two *meso* positions substituted with pentafluorophenyl and the other two *meso* positions are substituted with 4-phosphonated phenyl for surface binding and assembly formation. It was synthesized from 5-pentafluorophenyldipyrrylmethane and 4-(diethoxyphosphoryl)benzaldehyde by acid catalyzed condensation reaction. Metallation was carried out by treating the free base porphyrin with zinc(II) acetate.

Porphyrin-loaded nano-crystalline TiO_2 films were prepared by dipping ~7 m thick nano-crystalline TiO_2 films in a 1.2 mM solution of hydrolyzed porphyrin **1** or **3** in 1:1 CH_2Cl_2/MeOH mixture. Adsorption of the porphyrin to the slide was monitored over time with surface saturation reached in ~2 h. From the adsorption isotherm, a maximum surface coverage of 6.3 $\times 10^{-8}$ mole.cm^{-2} which is comparable to Ru-bipyridyl based chromophores.

Excited state energetics were estimated from solution phase electrochemistry and emission measurement. A simplified energy diagram is given in Figure 4.2. Emission quenching of both the free base and Zn-porphyrin derivatives bound to *nano*-TiO_2 was investigated in parallel with the porphyrin surface-bound in ZrO_2 films. A significant amount (~80%) of emission quenching is observed for the Zn-porphyrin bound to TiO_2 compared to ZrO_2 (Figure 4.3). However, almost no emission quenching was observed for free base porphyrin due to a lower excited state potential (-0.34 V vs NHE) of free base porphyrin than that of Zn porphyrin (-0.7 V vs NHE). However, on SnO_2 emission quenching is observed for both free base as well Zn-porphyrin (Figure 4.3).

A chromophore-catalyst assembly was prepared by previously demonstrated methods published from our group. . In these experiments, TiO_2 slides were dipped in solutions of **1** (1.2 mM in MeOH), $ZrOCl_2$ (5mM in 0.1 M $HClO_4$) and **2** (350 M in MeOH) successively for 4 h in each solution. Formation of assemblies was monitored by measuring absorption spectra of the slides (Figure 4.4). To check if the porphyrin formed a compact monolayer, a porphyrin-loaded TiO_2 slide was dipped in a solution of **2** and the change in absorption was observed within a 30 min time period. Absorption measurements on the resulting slides were consistent with co-deposition of **2** on surface-bound **1** but the extent of loading was small, not exceeding ~15% of the porphyrin loading as determined from absorption measurement and the increase in absorbance at 500 nm, a λ_{max} for the Ru(II) complex. The origin of the increased absorbance appears to be due to co-deposition of the Ru(II) catalyst directly on the electrode surface by surface phosphonate binding. Over extended periods, the extent of Ru(II) loading was observed to increase with concomitant decrease in porphyrin absorbance and the porphyrin was displaced from the surface.

By contrast, after dipping the porphyrin loaded slide in a $ZrOCl_2$-containing solution followed by the catalyst, a substantial change in absorption occurred consistent with formation of a –porphyrin-Zr-Ru(II) layer-by-layer structure. The absorbance at 500 nm was nearly

doubled after Zr(IV) treatment (Figure 4.4). Since both the porphyrin chromophore and the Ru(II) catalyst have comparable molar extinction coefficients from 450-700 nm, the absorbance doubling indicates formation of a 1:1 chromophore-catalyst assembly. Bilayer films of porphyrin and Ru(II) catalyst were similarly formed on nanocrystalline SnO_2 films with the absorbance behavior matched closely with that on TiO_2.

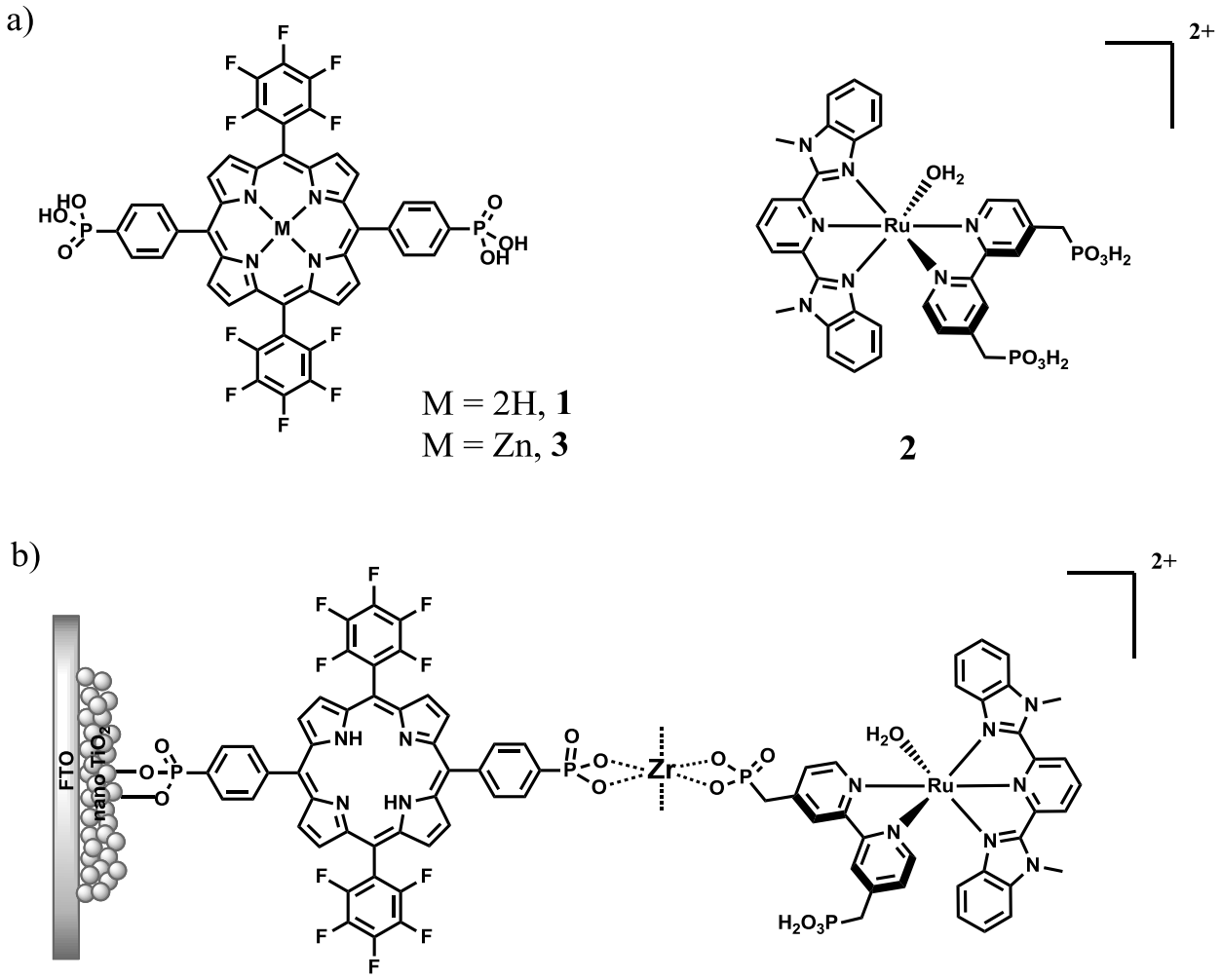

Figure 4.1. a) Porphyrin chromphores studied in this work and the appended water oxidation catalyst. b) Schematic representation of the bilayer chromophore-catalyst assembly

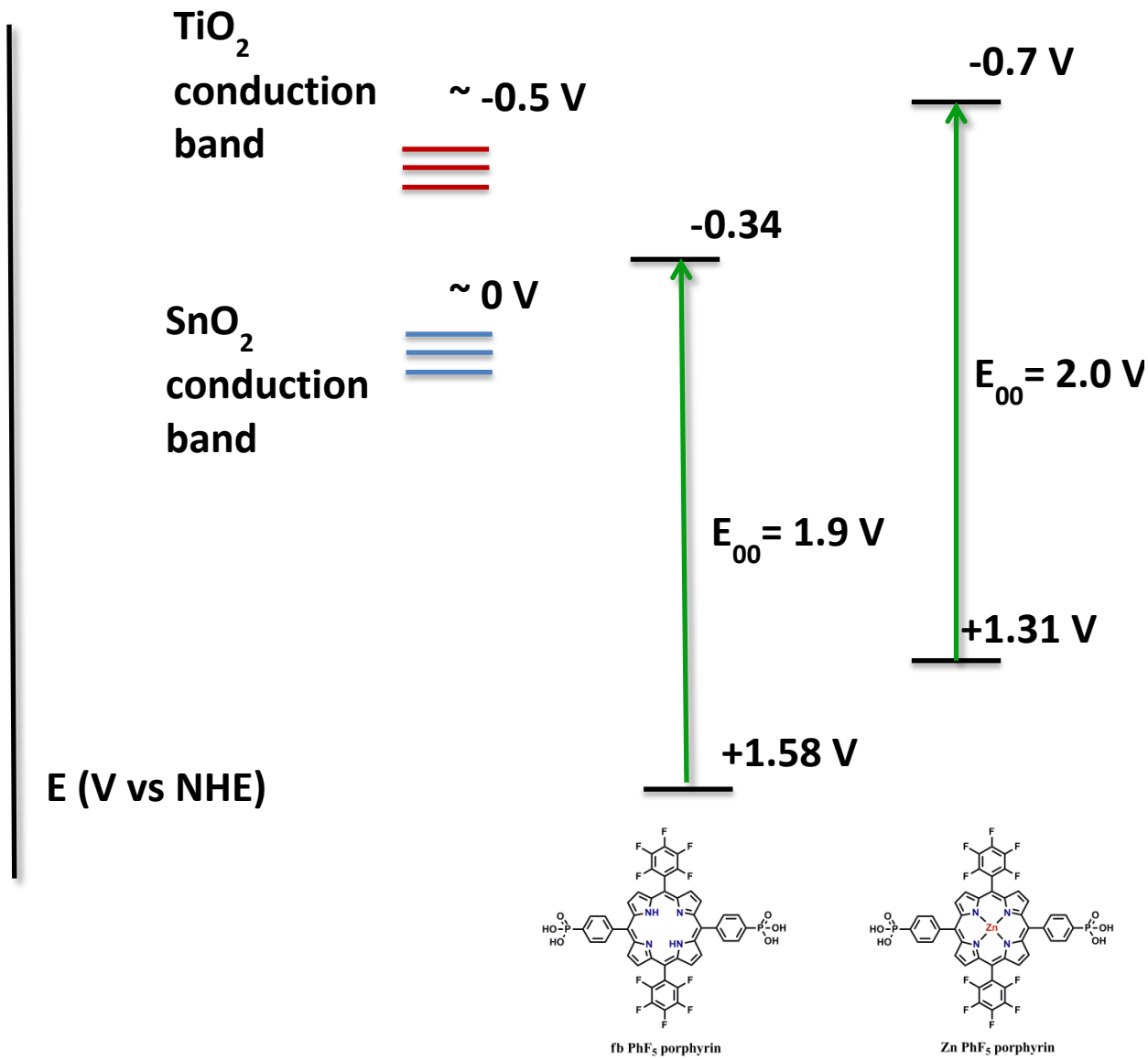

Figure 4.2 Redox potential level diagrams for the phosphonate derivatized porphyrins showing excited states suitable for injection into SnO_2 metal oxides.

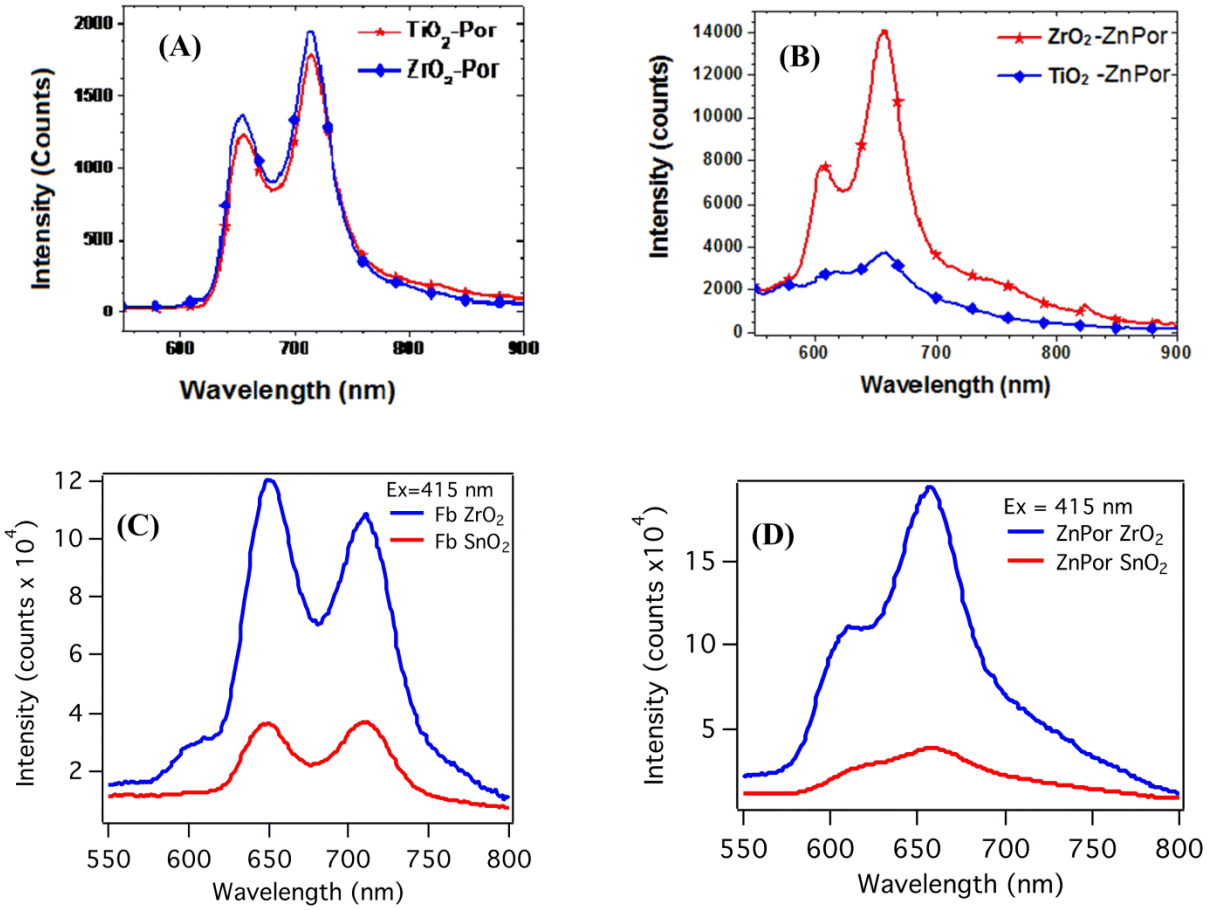

Figure 4.3 Emission quenching of porphyrin on metal oxides compared to ZrO_2.(A) free base porphyrin on TiO_2, (B) Zn(II)-porphyrin on TiO_2, (C) free base porphyrin on SnO_2 and (D) Zn(II)-porphyrin on SnO_2.

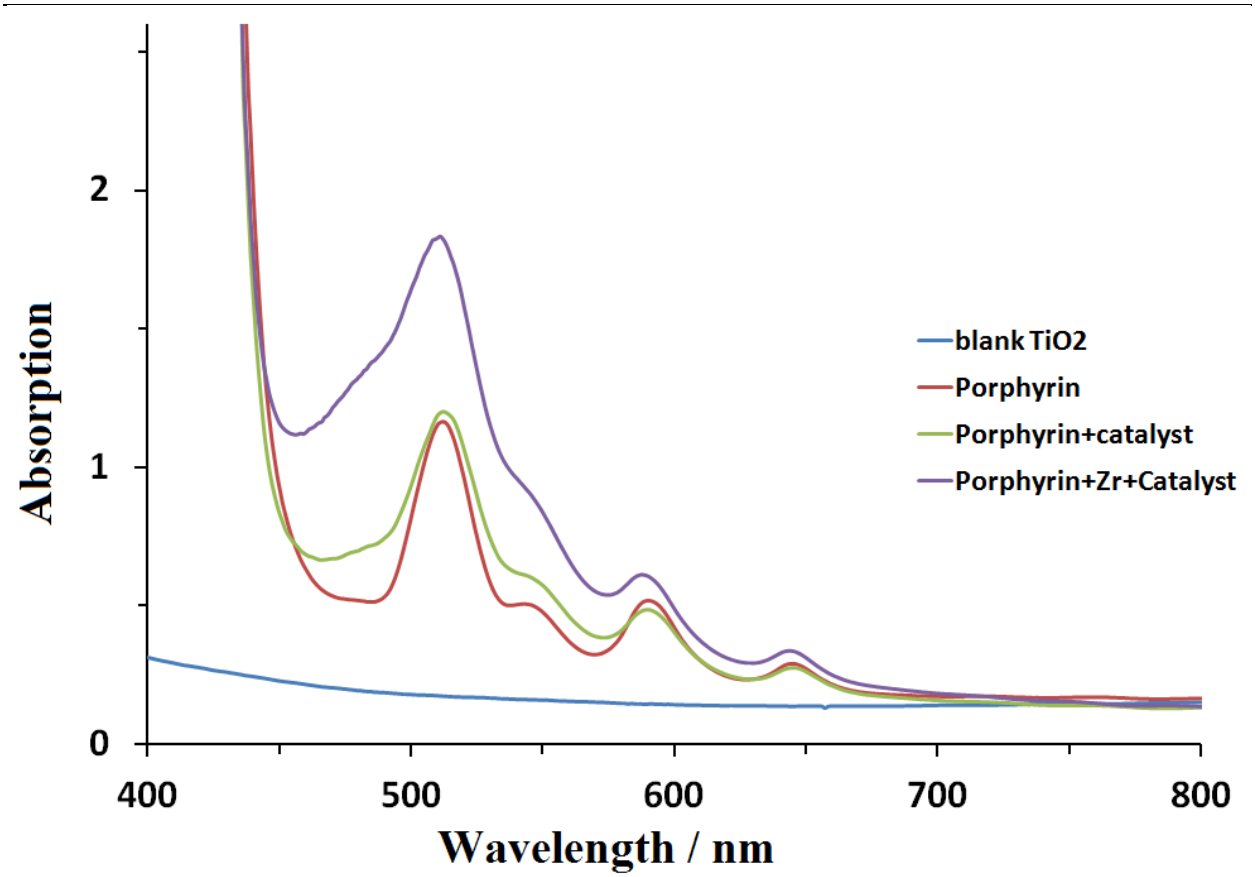

Figure 4.4. Absorption of bilayer assembly